Q. J. R. Meteorol. Soc. (1999), **125**, pp. 1959–1995

Aircraft observations of sea-breeze frontal structure

By R. WOOD*, I. M. STROMBERG and P. R. JONAS
University of Manchester Institute of Science and Technology, UK

(Received 13 February 1998; revised 14 September 1998)

SUMMARY

Detailed aircraft observations of sea-breeze frontal structure and dynamics are presented for two cases of well defined sea-breeze fronts near the east coast of England. In the first case the sea-breeze was advancing into a well mixed convective boundary layer with strong turbulence and an offshore breeze of around 3 m s^{-1}. In the second case the sea-breeze was penetrating into a convective boundary layer characterized by weaker turbulence and an offshore wind speed of 2–3 m s^{-1}. Indeed, during the course of the measurements a stable internal boundary layer was forming in the early evening. Cross-sections of the frontal structure are derived from aircraft traverses at a range of heights along a fixed line normal to the coast. A typical head-like structure is observed in both cases, with a region of strong mixing immediately seawards of the head. An approximately exponential fall-off in dissipation rate with distance seaward of the leading edge of the front is found. Heat and momentum fluxes are used to derive turbulent kinetic energy (TKE) budgets for the mixing region and indicate that turbulence in this mixing region is maintained by TKE generated by strong shear at the top of the cold-air inflow. In the first case the shear production of TKE is almost twice that of the second case, suggesting that the presence of ambient turbulence in the convective boundary layer has a significant effect upon the frontal dynamics. In the second case, as the turbulence decayed, a curious wave-like structure appeared behind the leading edge of the front. The waves have wavelengths of 1–3 km and it is unlikely that they were caused by Kelvin–Helmholtz instability. It is suggested that the waves might be a solitary wave-train emerging as the sea-breeze interacts with a low-level stable layer forming in the early evening.

KEYWORDS: Airborne observations Kelvin–Helmholtz instability Richardson number Sea-breeze front Turbulent kinetic energy

1. INTRODUCTION

A sea-breeze front is an atmospheric density current which occurs because of density differences between two adjacent air masses. This density difference is governed by the differential solar heating of the land and sea surface. The sea-breeze generally forms around the British Isles in the summer months, when the daytime land–sea temperature difference is at its greatest, and is manifested in an onshore low-level dense flow which undercuts the warmer air over land as it propagates inland. If the initial density difference is great enough a sharp frontal structure forms (Reible *et al.* 1993) with a raised head-like structure at the leading edge of the flow (Koshmieder 1936; Simpson *et al.* 1977). The frontal structure is most clearly defined in cases where the synoptic gradient wind is light and offshore (i.e. opposing the sea-breeze flow).

Much experimentation on gravity currents has been performed using laboratory tank models. Britter and Simpson (1978) used water with salinity differences to obtain differential densities and showed that a region of strong turbulent mixing forms immediately behind the frontal head which serves to detrain cold, dense fluid into the warmer fluid aloft. The mixing in the laboratory models is attributed to breaking Kelvin–Helmholtz (K–H) waves which form due to the wind shear at the head of the front. Although the laboratory models demonstrate many of the features observed in sea-breezes (Simpson and Britter 1980), the low Reynolds numbers obtainable (<few thousand) are insufficient to provide a precise laboratory analogue of the sea-breeze front although some research (Simpson and Britter 1979) suggests gravity current flows are independent of Reynolds number (Ri) for $Ri > 1000$. What is possibly more important is that an accurate representation of the effects of convective turbulence and cooling over the sea has not been achieved to date in laboratory models.

* Corresponding author, current affiliation: Meteorological Research Flight, Building Y46, DRA, Farnborough, Hants GU14 6TD, UK.

Atmospheric measurements of sea-breezes are relatively sparse, and airborne measurements rarer still. Simpson *et al.* (1977) used a glider, instrumented for the measurement of temperature, rate of climb, and humidity, to investigate the frontal characteristics of sea-breezes in the south of England, and demonstrated that there was a sharp frontal structure at the leading edge with a region of large temperature and humidity variation behind. It was not possible, with the limited instrumentation available, to say whether the mixing was instigated by K–H instability. Observations of thunderstorm outflows, using dual Doppler radar (Mueller and Carbone 1987), show that K–H billows are formed in many cases, although in each case-study (a) the gust front was propagating through a stable boundary layer, and (b) the speed of the fronts observed was substantially greater than most sea-breeze fronts.

Kraus *et al.* (1990) provided the first detailed dynamical measurements of the sea-breeze using a GROB G109B aircraft instrumented for high-frequency measurement of the three components of wind velocity, temperature and humidity. Front-normal cross-sections were constructed from numerous runs through sea-breezes at various heights, and the processes of frontogenesis and frontolysis were investigated. A major finding was the importance of the effect of confluence on the frontogenesis, and the effect of the synoptic wind in increasing the gradients of humidity and potential temperature. Shear processes were also found to be important in the generation of frontal lobes and clefts.

Numerical studies provide some interesting insights into the processes occurring at the leading edge of a sea-breeze front. A two-dimensional, non-hydrostatic, compressible model (Sha *et al.* 1991) was used to investigate in detail the interaction of the sea-breeze with convective processes, which were explicitly resolved in the model. The model also provided evidence for the production of K–H instabilities at the foremost part of the head which were found to be responsible for the entrainment of upper air into the sea-breeze, and also for increasing the friction at the top of the gravity current, resulting in a slowing of the propagation speed during the middle of the day. A fine-scale numerical model by Liu and Moncrieff (1996) ratifies some of the earlier laboratory-tank-model findings concerning the effect of the ambient wind upon the form and structure of the gravity current head, in that a headwind (opposing the sea-breeze flow) raises the head of the gravity current relative to the following feeder flow while a tailwind flattens it.

This paper presents detailed observations of two sea-breeze fronts close to the east coast of England, using a light aircraft instrumented for the measurement of wind, temperature and humidity. The first set of observations is of a sea-breeze penetrating into a boundary layer characterized by strong turbulent mixing. The second set of observations was carried out in the early evening as a convective boundary layer weakened, and a stable layer began to form close to the surface. Section 2 contains a description of the instrumentation, background to the observations and geographical location. Sections 3 and 4 give details of the case-studies. Conclusions and inferences are addressed in section 5.

2. Instrumentation and background to observations

(*a*) *Wind, temperature and humidity measurement*

Data were taken using a Cessna-182 aircraft owned and operated by the Department of Physics at the University of Manchester Institute of Science and Technology (UMIST). The aircraft instruments measure the three wind-velocity components, temperature and humidity. The wind measurements are made at a frequency of 20 Hz

using a five-hole gust probe and an accelerometer system, with Global Positioning System (GPS) data to correct long-term drifts in the accelerometer measurements. Absolute accuracy of the measured winds is 1–2 m s^{-1} for the horizontal components and 0.25 m s^{-1} for the vertical wind component. Horizontal wind measurements are corrected using reciprocal wind-calibration runs (Offiler *et al.* 1994) which in this study results in a typical along-track wind component accuracy of better than 1 m s^{-1}.

Temperature was obtained by using a Rosemount total temperature probe corrected for adiabatic heating effects using a recovery factor determined from flight tests. The time-response of the temperature probe is around 1 s, and data are logged at 1 Hz. Absolute accuracy of the temperature probe is typically 0.2 degC, with a relative error of around 0.05 degC. Humidity measurements were made using a Mitchell cooled-mirror dew-point hygrometer. The measurements are logged at 1 Hz. A complete description of the instrumentation is found in Wood *et al.* (1997).

For straight and level runs the aircraft wind, temperature and humidity time-series data are transformed into spatial series by interpolation onto equally spaced points on a straight line parallel to the aircraft track over ground and fixed in space. The precise start and end points of the line are determined by the user so that several approximately coincident aircraft runs can be consistently interpolated onto a vertical plane. The interpolation also minimizes errors to the flux measurements caused by having, for example, poorer spatial sampling of updraughts (higher air speed resulting from the operation of the aircraft at constant power) than downdraughts (lower air speed). Since the aircraft has a spatial sampling resolution of between 2.4 and 3.2 m depending upon air speed, a grid spacing of 2.5 m along the interpolating line was chosen.

(*b*) *Flux measurements*

Variance and flux measurements were carried out using the eddy correlation technique. The product of the fluctuating quantities is obtained directly from the spatial series after first removing the mean and linear trend of each spatial series. The absolute accuracy of the measurements does not thus preclude accurate flux measurements. Random (sampling) errors, however, are typically large, especially in the boundary layer. Errors in fluxes involving the product of two different wind velocity components are especially high owing to the large integral scale that such products generally have in the boundary layer and the lower correlation coefficient generally observed between the horizontal and vertical wind components than the vertical wind component and temperature. Random errors were calculated by means of an integral scale derived using autocorrelation functions (variances) and cross-correlation functions (fluxes) of the spatial series (Lenschow and Stankov 1986). As such they are environment dependent and range from 10–100% (buoyancy flux) and 30–200% (momentum fluxes). Multiple sampling can improve this accuracy, although care must be taken in the selection of relatively statistically homogeneous regions in which averaging is appropriate. Systematic loss of covariance at high frequency is a possible problem when detrending short time series to ensure homogeneity. The ratio of the length of series L and the integral scale λ of a certain variable was used to assess the magnitude of this problem (Lenschow *et al.* 1994). For the convective boundary-layer series in this study this is likely to lead to a loss of vertical wind variance of 2–9% and loss of sensible-heat flux of 1–7%. For series in the head region of the sea-breeze the losses of vertical wind variance and sensible-heat flux are 2–10% and 1–5% respectively. These systematic losses are relatively small when compared with the random error involved in the measurements.

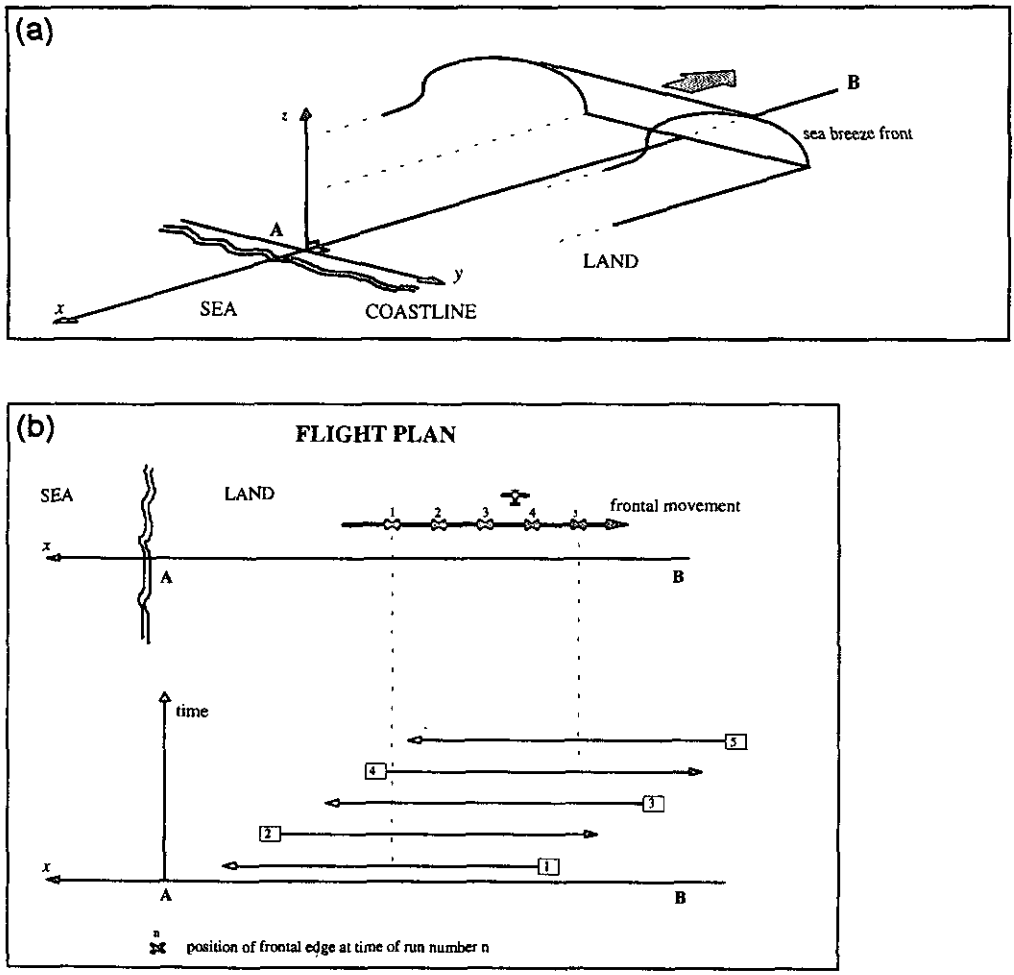

Figure 1. (a) Details of the coordinate system used in this study. The sea-breeze is depicted as moving inland parallel to the x-axis with the y-axis parallel to the leading edge of the front. Points A and B on the x-axis define a line along which the aircraft runs are made at a range of heights z. (b) A schematic of the flight, detailing how the aircraft runs move progressively further inland as the front moves inland so as to cross the leading edge of the front approximately halfway along each aircraft run.

(*c*) *Flight plans and location of measurements*

Figure 1 depicts the sea-breeze front and coordinate system used. The flight pattern involves making straight and level runs in a *front-normal* direction at a range of altitudes from around 200 m above mean sea level (a.m.s.l.) up to an altitude of 1500 m a.m.s.l. above the inversion. In order to construct vertical cross-sections of relevant parameters the runs should all be aligned along a constant track over the ground (line AB on Fig. 1). Because the position of the sea-breeze front is moving with time in the direction AB the start position of each run becomes further from point A with each run so the position of the frontal edge divides the run into roughly equal parts, as shown in the x–time plot of Fig. 1. The runs are shown as starting and ending at the same time only to aid clarity.

For the runs along the line AB, all data are interpolated using GPS data onto the vertical plane containing the line AB and the altitude coordinate. After interpolation

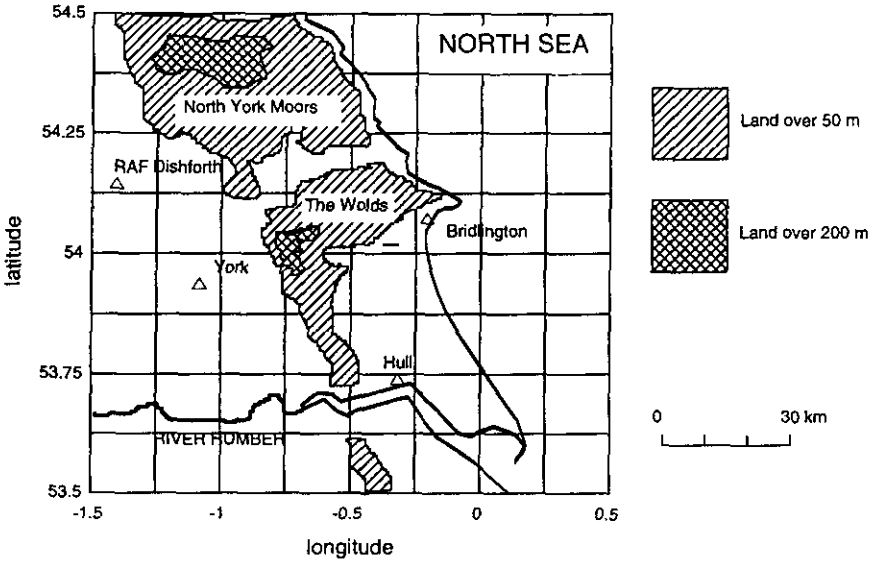

Figure 2. Locale of the aircraft measurements on the east coast of England. The measurement area for the two flights was the hinterland of the relatively straight coastline between Bridlington and the River Humber estuary.

onto this plane the data are a function of the distance x along the line AB and the altitude above sea level. Using surface elevation data obtained from a topographic map of the area, each height value is transformed to a height above the surface. The x coordinate of the front, as measured on each run, will vary between runs for two reasons: the front is moving; and the frontal surface is not a vertical surface, at a fixed time it slopes seaward with height above ground. To align the runs into a front-relative coordinate, the speed of advancement of the front must be known. Two or more runs close together in height are used to derive the speed of the front, U_{front}, at that particular height. The frontal edge is clearly defined by a sharp jump in temperature, ΔT, and a corresponding sharp drop in dew-point, ΔT_{d}. The position of the frontal edge was defined to be located at the position where the temperature is $T_{\text{land}} - 1/2\Delta T$, where T_{land} is the temperature immediately to the landward side of the temperature drop. It is then assumed that the speed of the front is the same at all altitudes, which is reasonable if the front is in approximate equilibrium. This frontal speed is then used to shift the x coordinate of the remaining runs to remove the motion of the front and render the data in a front-relative coordinate x'. In each case x' is zero at the frontal surface at the height used to derive the speed of the front, positive seawards and negative landwards. The observations of sea-breeze fronts were made close to a section of the east coast of England (Fig. 2) between the River Humber estuary (0°12′E, 53°36′N) and Flamborough Head (0°6′W, 54°6′N), a region with a relatively linear coastline and prosaic hinterland.

3. Case A–25 June 1996

(a) *Synoptic situation and boundary-layer profiles*

Conditions on 25 June 1996 were dominated by an anticyclonic high-pressure system that had moved in from the west over the previous two days. The high pressure brought high land temperatures and light winds, ideal for the formation of sea-breezes and a daytime convective boundary layer approximately 1000 m deep. Over much of

eastern England, on 25 June, offshore winds of around 3–4 m s^{-1} began early in the morning as the overnight nocturnal boundary layer was broken down and convective thermals began to form at around 0900 h (local time = GMT + 1 hour). The temperature quickly increased from around 10 °C overnight to a maximum of 23 °C at RAF Dishforth at 1230 h. A sea-breeze front began to develop at around 1100 h shortly after the first strong thermals had started to form.

Two profiles were taken by the aircraft and are shown in Fig. 3. The profile on the landward side of the front (1445 h) shows the presence of a well mixed boundary layer up to a height of 1000 m with almost constant values of potential temperature and specific humidity. At 1000 m there is a sharp inversion with a 1 degC step in potential temperature. Above the inversion is a stable layer with a potential temperature lapse rate of 7.5 degC km^{-1}. The coastal sounding (1515 h) shows a less well mixed layer with a shallow gradient of potential temperature of 1.9 degC km^{-1} from 600 m up to the main inversion at roughly 1300 m. The inversion is greater in magnitude, but less sharp, than the inversion over the land, with a 4 degC rise in potential temperature over a vertical distance of 150 m. Above the inversion is a stable layer up to an altitude of 1700 m where there appears to be a second smaller inversion. The lapse rate in this layer is 1.5 degC km^{-1} giving a Brunt–Väisälä frequency of 0.007 s^{-1}. The coastal sounding also reveals the presence of a layer between 300 and 450 m which is warmer than the air both above and below it by 1–2 degC. Below 300 m is a stable layer which can be attributed to cold sea air forming the sea-breeze feeder flow. The warm layer above could be attributed to the sea-breeze return flow which contains a mixture of land and sea air.

(*b*) *Aircraft runs*

A line of cumulus clouds running approximately parallel to the coast marked the enhanced uplift at the sea-breeze front. The seaward side of the front was clear except for some patchy dissipating cumulus close behind the front. Upon reaching the coast a GPS fix (fix A) was taken and the aircraft turned through 170° to fly back normal to the front at the same altitude. A second GPS fix (fix B) was taken approximately 10 km to the landward side of the line of cumulus. The two fixes were then used to direct all the subsequent traverses of the frontal zone. The flight tracks are shown in Fig. 4 with the GPS fixes shown. The initial run towards Bridlington from Dishforth constitutes run 1 although it is displaced to the north of the subsequent runs by around 5 km.

Thirteen more traverses were made at a range of altitudes from 350 m to 1555 m a.m.s.l. Run altitudes were chosen so as to obtain as much vertical resolution as possible in the lowest 800 m of the boundary layer. This would enable cross-sections through the sea-breeze front to be built up from the data. In addition, a run just below the inversion and a run at 1550 m were made to investigate any influence of the lower-level sea-breeze flow upon the inversion and the free atmosphere respectively.

(*c*) *Alignment of runs, spatial series, cross-sections and vertical structure*

GPS fixes at the start and the end of each run were used to calculate a single linear track AB on the ground onto which spatial series were resolved. Run 1 was excluded from this process since it is aligned some 5 km to the north of the line AB. The position of the front x, as defined as the distance from the coast along the line AB, is shown as a function of time in Fig. 5, and is approximately linear. The frontal speed was obtained from runs 4, 7 and 14 (where in each case the height above ground at the frontal surface was between 290 m and 300 m), and gave a frontal speed of 1.25 m s^{-1}, which was used

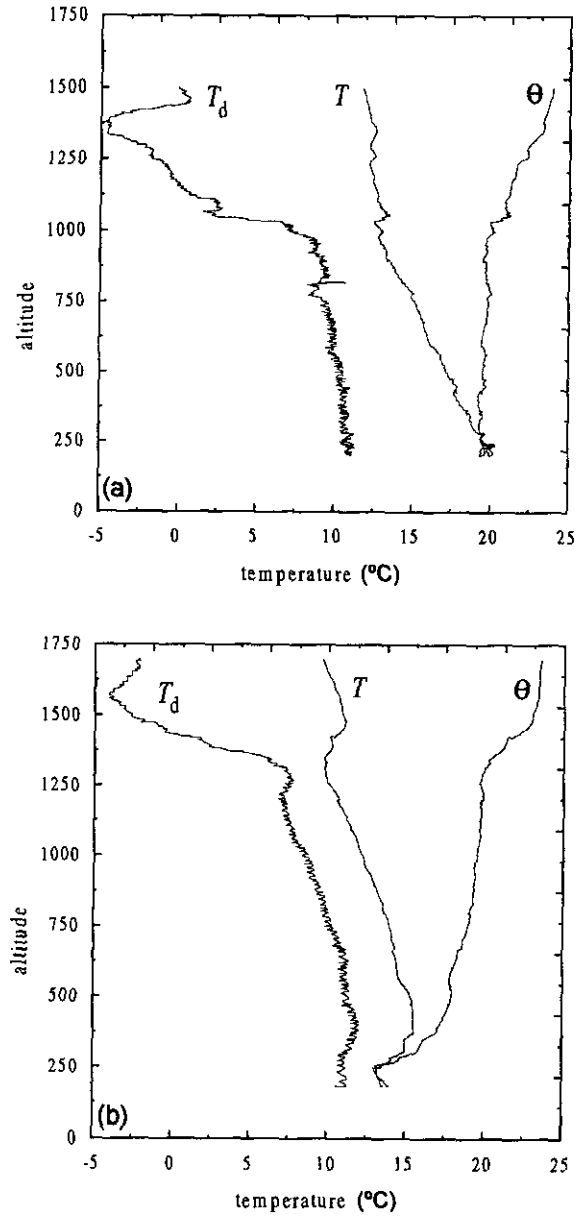

Figure 3. Profiles of temperature T, potential temperature θ, and dew-point T_d taken by the aircraft on 25 June 1996 (a) at 1445 h and (b) 1515 h. Altitudes are given as metres above mean sea level. The profiles were made in (a) the convective boundary layer landward of the sea-breeze front which shows a well mixed boundary layer capped by an inversion at 1000–1100 m, and (b) close to the coast with the front around 20 km inland which shows a low-level cold inflow below around 300 m. Above the inflow region a relatively stable layer extends up to a capping inversion at around 1300 m.

to transform all the runs into the front-relative coordinate x'. The resulting positions of the front from all the frontal traverses as functions of height above ground are shown in Fig. 6 (crosses). There is considerable scatter in the frontal position with height which is probably due to both a nonlinear progression of the front on the small scale, and because the frontal surface does not move as a rigid body, but is constantly being shifted. Indeed, evidence of this has been found in a shifting lobe and cleft structure

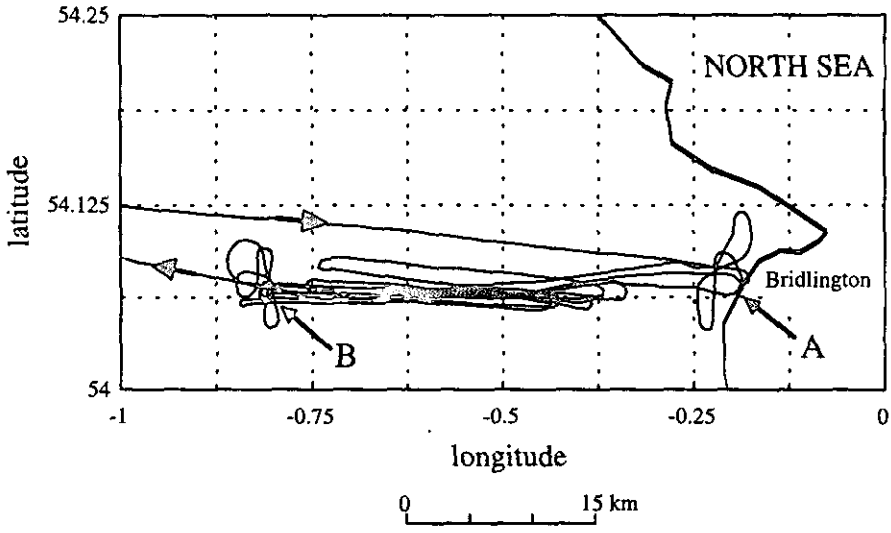

Figure 4. Aircraft flight track for 25 June 1996. A total of 14 runs were flown in a direction normal to the line of the sea-breeze front which was defined clearly by a line of enhanced convective clouds running north–south. The points A and B are used to define a reference track onto which the aircraft data are resolved.

observed in laboratory tank models (Simpson 1972), and atmospheric density currents (Lawson 1971). Nevertheless, averaging the position–height data into roughly 100 m height bands, as shown by the dashed line and circles in Fig. 6, yields a frontal structure that is steepest close to the ground and becomes shallower with height. The slope of the front is around 30° to the horizontal below 500 m height. Hacker *et al.* (1990) found frontal slopes closer to 10° from aircraft measurements of sea-breezes in Australia, although the offshore synoptic wind component during their observations was greater at 7–10 m s^{-1}. Simpson and Britter (1980) examined the effect of varying the magnitude of the opposing flow in laboratory density currents and showed the frontal surface to flatten significantly as the speed of the opposing flow is increased.

Aligned spatial series of vertical velocity, potential temperature, specific humidity and wind speed parallel to the line AB (positive offshore) are shown as functions of x' in Figs. 7(a) to (d). Each figure displays six series at a range of heights from 215 m to 1430 m above ground level in order to gain insight into the frontal characteristics with position relative to the front. For all the series below the inversion (1000–1200 m) the strong convection on the landward side of the front is particularly noticeable in the vertical-velocity series. Convective cells are on the kilometre horizontal scale with maximum updraughts of around 4 m s^{-1}. The sea-breeze front is clearly marked by a sharp decrease in temperature and a sharp increase in specific humidity. The horizontal position of the front is marked as the dotted line separating regions 'a' and 'b'. From the temperature series at $z = 800$ m there is a drop in temperature between $x' = 1650$ m and $x' = 2440$ m, but the temperature at $x' > 1650$ m remains typical of the temperatures to the landward side of the frontal region. The lower temperature in this narrow cold region probably results from mixing of the sea and land air at the frontal edge itself, and that some of the mixed air has been carried upwards at the broad frontal updraught. A broad frontal updraught is present extending 200–1000 m to the seaward side of the front and 500–2000 m to the landward side of the front. The presence or absence of convective updraughts amplifies or reduces the magnitude and horizontal extent of the updraught region. An onshore breeze is observed in the wind speed parallel to the line

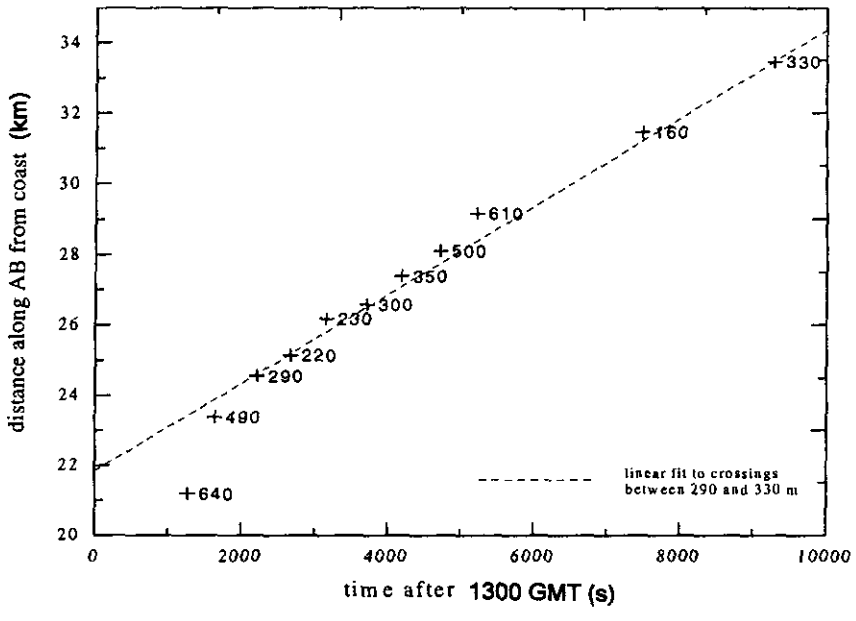

Figure 5. Position of the leading edge of the front as a function of time after 13:00 GMT on 25 June 1996. The position is given as the distance in kilometres from the coast along the line AB (see Fig. 4). The numbers adjacent to each point give the height above ground of the frontal crossing.

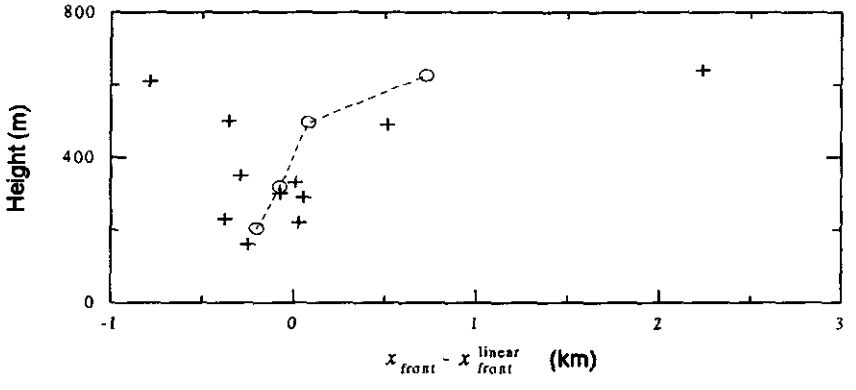

Figure 6. Measured minus linear fit position of the front against altitude. For details see text.

AB below $z = 335$ m. There appears to be some enhancement of the offshore synoptic flow as it flows over the denser sea air beneath. This is particularly noticeable in the runs at $z = 660$ m and $z = 800$ m, and could be evidence of a sea-breeze return flow, as onshore sea air is lifted up into the head of the sea-breeze and forced seawards above the cool-air inflow. It is likely that the synoptic flow over the dense sea-breeze is subcritical in nature. The Froude number, Fr, is given by

$$Fr = \frac{U}{(g'h)^{1/2}}, \tag{1}$$

where $g' = g\Delta\theta/\theta$ is the reduced gravity (θ being the potential temperature), U is the speed of the front relative to the ambient synoptic flow and h is the depth of the

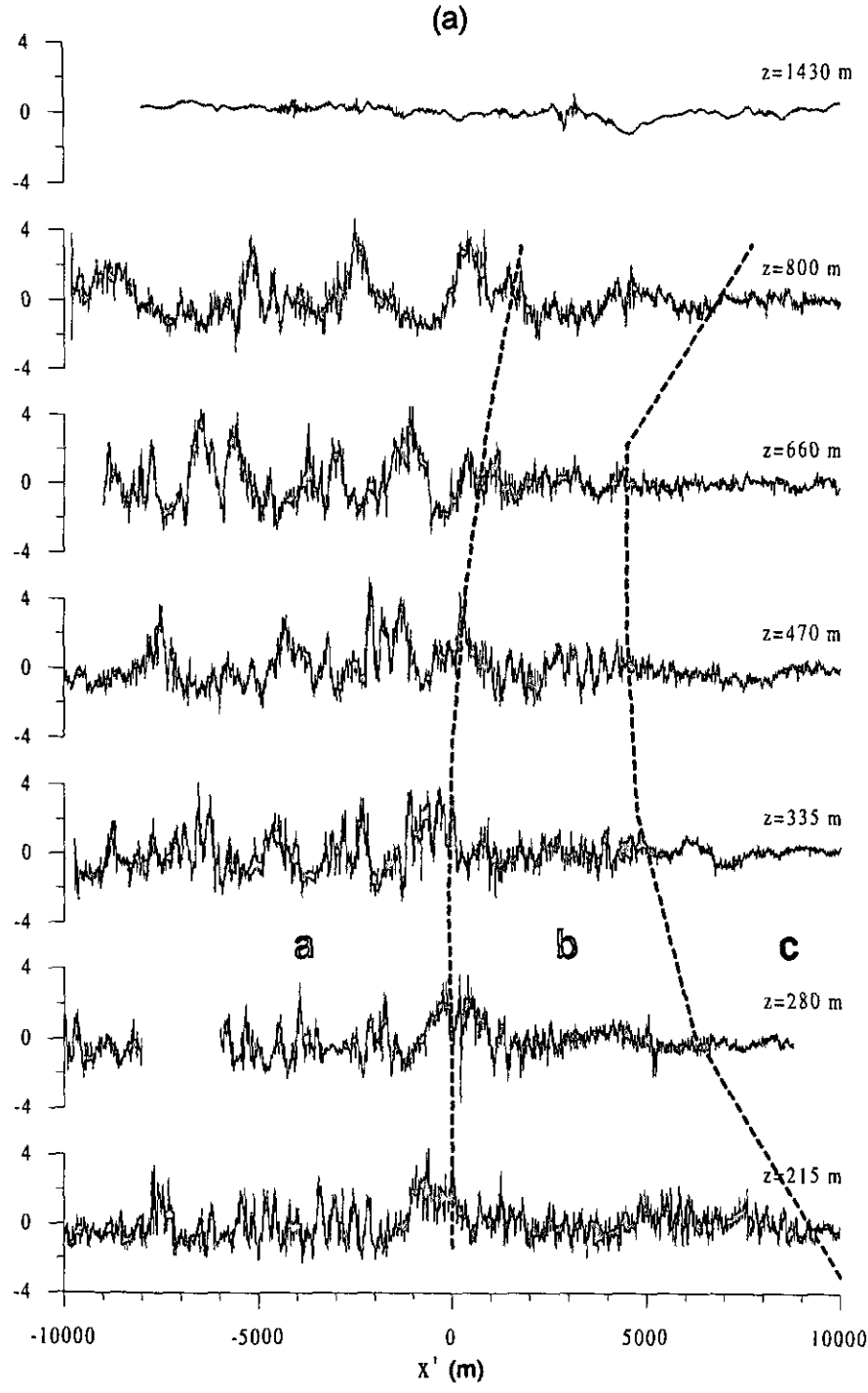

Figure 7. Aligned spatial series of (a) vertical velocity (m s^{-1}), (b) potential temperature (°C), (c) specific humidity (g kg^{-1}) and (d) front-normal wind speed (m s^{-1}) (positive for offshore) from seven of the aircraft runs at different heights, z, on 25 June 1996. The runs have been shifted along the line AB (see Fig. 4) using the coordinate transformation described in the text. The regions 'a', 'b' and 'c' represent areas of different dynamical structure in the vicinity of the front (see text).

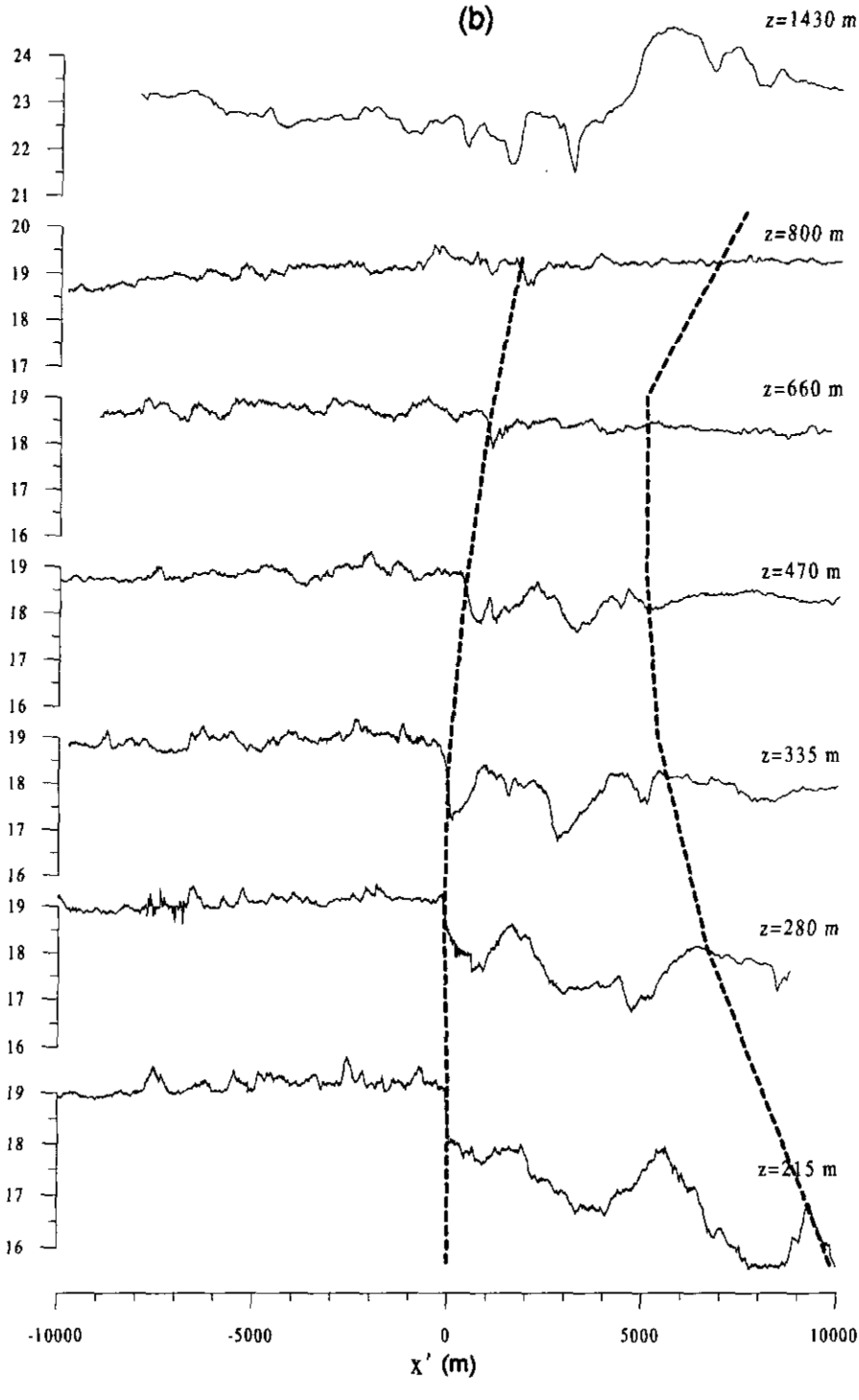

Figure 7. Continued.

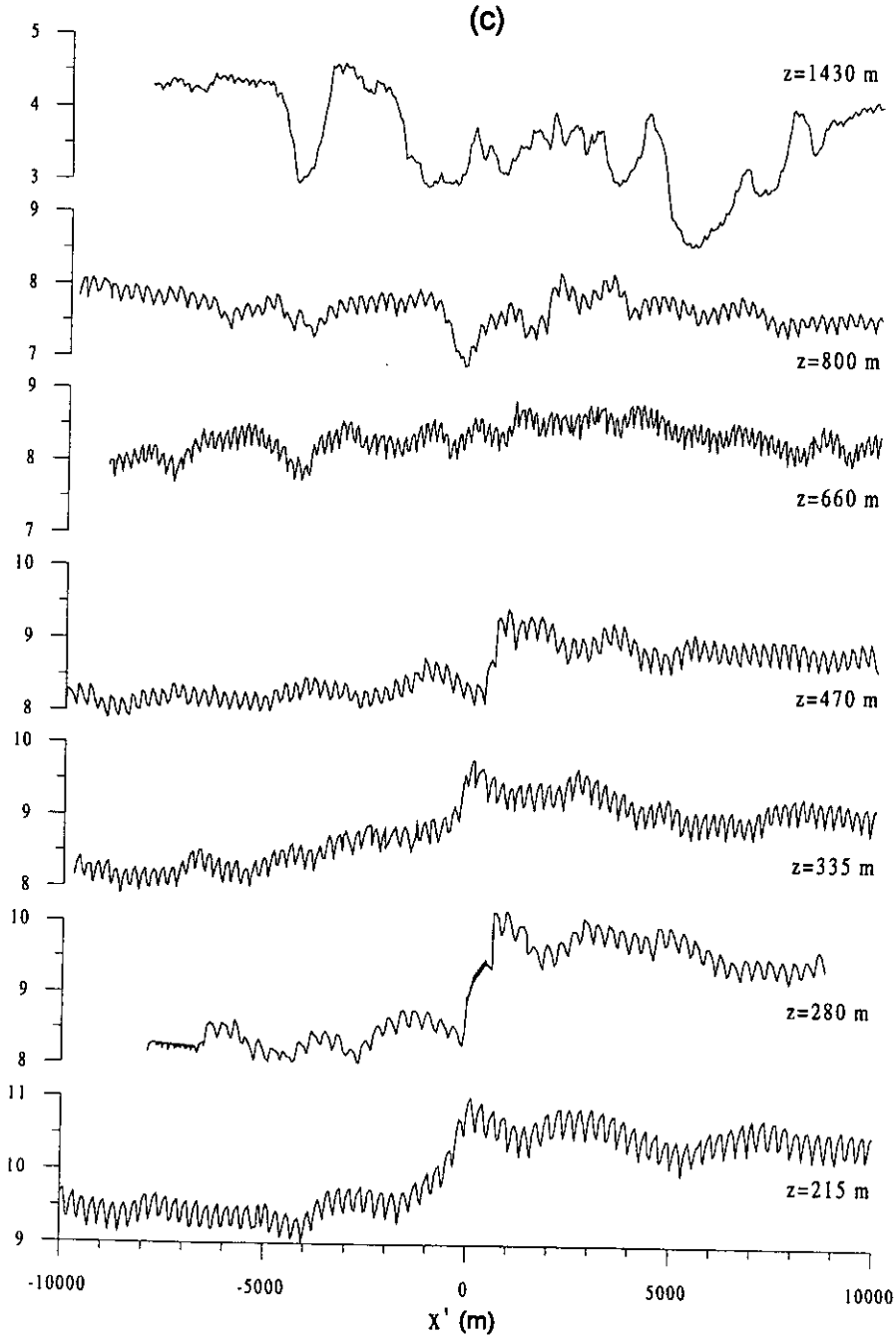

Figure 7. Continued.

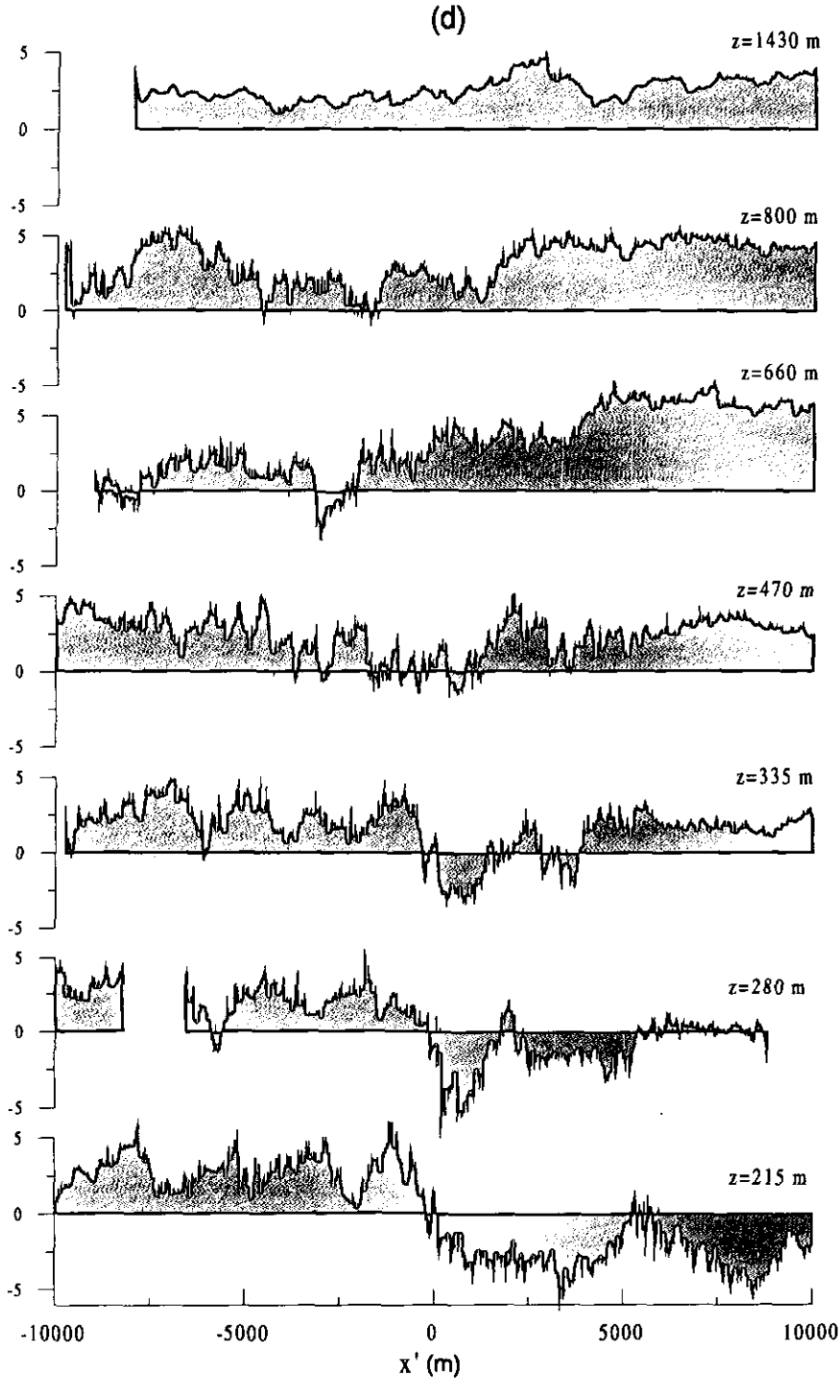

Figure 7. Continued.

sea-breeze inflow, which increases from subcritical values (0.78–0.85) immediately landward of the leading edge of the front to supercritical values (1.02–1.14) above the cold-air inflow for $x' > 5$ km—a result of the increase in offshore wind component above the cold air.

A second clear boundary in the flow is observed in the aligned spatial series of vertical velocity and potential temperature and is marked by the dotted line between the regions 'b' and 'c'. The boundary marks a distinct difference in the statistical nature of the vertical motion, with a sharp decrease in turbulence upon passing from 'b' (the head region) to 'c' (the inflow region).

This marked decrease in turbulence intensity is used to define the boundary and is observed at all altitudes from $z = 215$ m to at least $z = 660$ m. The boundary is less distinct at $z = 800$ m. The horizontal position of the boundary is between 4.5 and 9.5 km seaward of $x' = 0$ (the horizontal position of the leading edge of the front at the lowest aircraft level). The distance of the boundary from the leading edge is greatest close to the surface and is a minimum at an altitude between $z = 470$ m and $z = 660$ m. In the potential-temperature series the boundary separates large potential-temperature fluctuations on scales upward of a kilometre and a smooth, relatively homogeneous potential-temperature field. This boundary has been observed by Simpson *et al.* (1977) using measurements of potential temperature, specific humidity and more tenuously in the glider's variometer reading which is a measure of the vertical motion of the air. The vertical air measurements, however, were made at a sampling rate of only 1.6 Hz, equivalent to a measurement approximately every 50 m, and so do not reveal the sharpness of the boundary. The specific-humidity series show oscillations on the scale of a few hundred metres, resulting from the poor time response (several seconds) of the dew-point hygrometer.

Cross-sections in the x'–z plane of vertical velocity, wind speed along AB, potential temperature and specific humidity are shown in Fig. 8. The data from all the runs were interpolated onto a fixed grid with 100 m horizontal spacing and 25 m vertical spacing to produce the contour plots. The resolution was limited essentially for computational speed. The frontal head is clearly seen extending to a height of around 500–600 m, and the cold-air inflow extends to a height of around 300 m for $x' > 6$ km. A raised frontal head extends from $x' \approx 0$ to $x' \approx 6$ km and appears to consist of two separate raised regions rather than the classical single raised head. Landward of the front, convective thermals are marked most clearly by regions of updraught and downdraught. Seaward of the frontal region, above the cold-air inflow, the convective thermals are almost totally eliminated and a stable stratification is observed in the cross-section of potential temperature.

Figure 9 shows a wind vector plot of the u–w wind field. The potential temperature cross-section is also shown. Several important features are observed. First, the increase in the synoptic wind speed above the inflow is clearly seen. Second, a well defined updraught is present extending throughout the boundary layer in a region around a kilometre wide immediately landward of the leading edge of the front. Third, immediately seaward of the first raised cold region there is a downdraught region. Warm air from the synoptic flow above the sea-breeze appears to be entraining into the colder flow. Fourth, for $z > 700$ m and -2 km $< x' < 5.5$ km, waves with a horizontal wavelength of 3–4 km are present in the flow field. These waves are likely to be gravity waves generated in the stably-stratified offshore flow above the cold-air inflow, although it is interesting to note that the waves extend some distance 'upwind' of the sea-breeze.

Data from the grid obtained in the generation of the cross-sections were used to construct vertical profiles through the front. Figure 10 shows derived profiles of potential

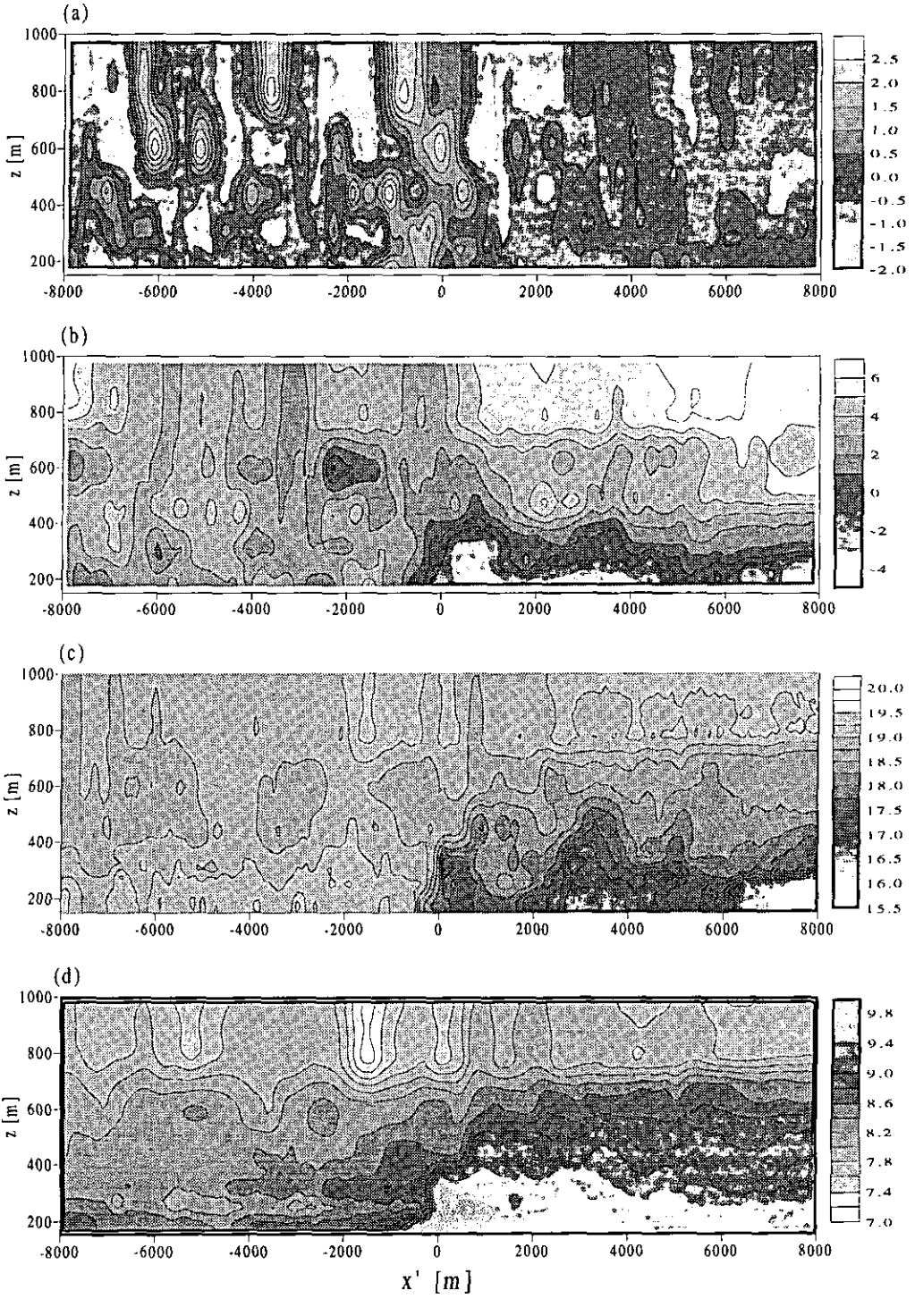

Figure 8. Cross-sections of (a) vertical velocity (m s^{-1}), (b) front-normal wind speed (m s^{-1}), (c) potential temperature (°C), and (d) specific humidity (g kg^{-1}) from the runs on 25 June 1996. The sections clearly show a raised frontal head extending to 500–600 m height and around 5 km seaward of the leading edge of the front. Seaward of the raised-head region a cold-air inflow extends to a height of 300 m.

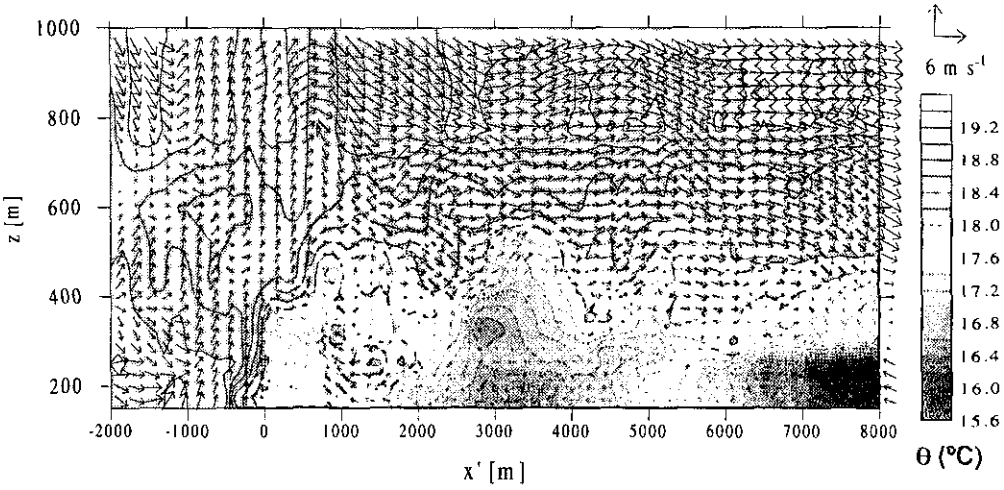

Figure 9. Cross-section of potential temperature with wind vectors (front-normal and vertical components) superimposed from the runs on 25 June 1996. A broad updraught is observed ahead of the front. Enhancement of the offshore synoptic wind is observed above the sea-breeze and there is evidence of gravity waves, probably triggered by the frontal updraught, moving into a stably-stratified region above the cold-air inflow.

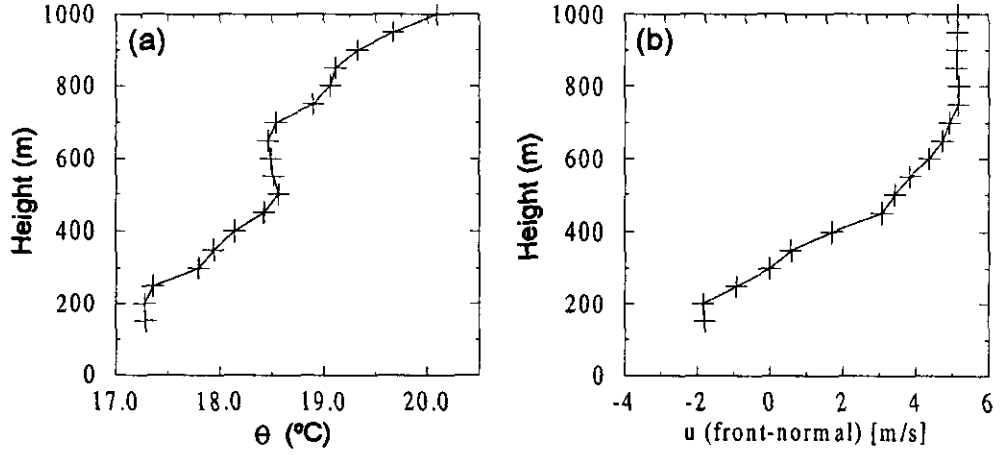

Figure 10. Profiles of (a) potential temperature, θ, and (b) front-normal wind speed, u, derived from the cross-sections of Fig. 8, for $0 < x' < 8$ km. A statically stable profile is observed above the sea-breeze (Brunt–Väisälä frequency ≈ 0.01 s^{-1}). A region of strong wind shear (0.025 s^{-1}) extends from $z = 200$ m to around $z = 500$ m, above which a weaker wind shear is present.

temperature and front-normal wind speed. These are average profiles taken from the cross-sections for 0 km $< x' <$ 8 km in and above the cold air. The potential temperature above 250 m is generally statically stable apart from a layer 200 m thick between 500 m and 700 m height where a neutral layer is found. The strongest wind shear (0.025 s^{-1}) is observed between 200 m and 500 m height. Above this a weaker shear exists up to around 700 m and the wind speed is constant with height above 700 m. Figure 11 shows a vertical profile of the gradient Richardson number (Ri) calculated using cubic spline fits to the potential temperature and front-normal wind-speed-profile data. Ri is small ($Ri < 1$) in a layer between 200 m and 600 m and falls below the critical value

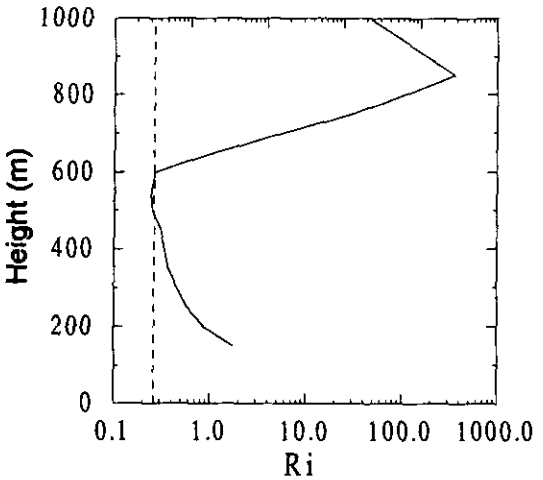

Figure 11. Vertical gradient Richardson number (Ri) profile derived from the profiles of Fig. 10. The vertical dashed line is the line $Ri = 0.25$ below which Kelvin–Helmholtz modes are unstable. Ri is plotted on a logarithmic axis to encompass the large range of values.

($Ri = 0.25$) for the formation of unstable K–H waves between 500 m and 600 m. The low Richardson numbers found suggest that K–H waves are breaking at the top of the cold-air inflow. The horizontal wavelength λ_{KH} of the most unstable K–H mode, and thus the most likely to be observed, is related to the thickness h of the layer where $Ri < 0.25$ and is shown (Turner 1973) to be in the range $6.3h < \lambda_{KH} < 7.5h$. This would suggest that the most dominant K–H mode has a value of $\lambda_{KH} = 630$–750 m, although it was found that the unstable layer thickness was sensitive to the use of different fits (e.g. polynomial fits) to the profile data, and that only a very broad estimate of 300 m $< \lambda_{KH} <$ 1000 m could be attained.

Further evidence for the production of K–H waves is shown in Fig. 12 which shows spatial series of vertical wind component, temperature and front-normal wind speed from a section of an aircraft run through the head region at $z = 470$ m. A five-wavelength train of waves is seen clearly in the vertical wind. Less well defined waves are observed in the front-normal wind component, and although some oscillatory behaviour is present in the temperature data no well-defined waves are seen. It is not known why no temperature waves are seen although it is possible that wave breaking in this region has caused mixing, resulting in a smoothing of the temperature gradients locally. The horizontal wavelength of the vertical wind waves obtained using a sinusoidal fit to the portion of the vertical wind data between the vertical dashed lines gives $\lambda_{KH} = 390$ m, consistent with the expected wavelength from the Ri analysis.

(*d*) *Dissipation rates*

A measure of the high-frequency fluctuations $\chi = (\mathrm{d}w/\mathrm{d}t)^2$ was calculated from the vertical wind data, w, following Meneveau and Sreenivasan (1991) and this is normalized to the run mean $\overline{\chi}$. Values of $\chi/\overline{\chi}$ are shown in Fig. 13 for the same set of aligned runs as Fig. 7. The intermittent nature of the high-frequency fluctuations is very clearly borne out, with peak values exceeding the mean in places by as much as two orders of magnitude. The χ values are particularly strong ahead of, and close to, the leading edge of the front, and decrease markedly with distance seaward of the front.

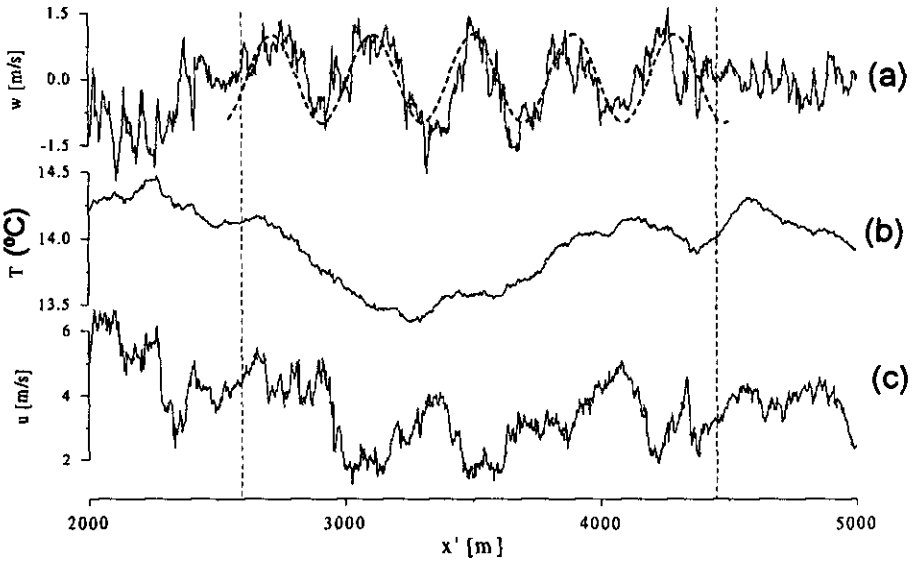

Figure 12. Spatial series of (a) vertical wind component, (b) temperature and (c) front-normal wind speed from a run at $z = 470$ m demonstrating the presence of a five-wavelength train of what are most likely Kelvin–Helmholtz waves. The dashed line is a sinusoidal fit to the vertical wind data with a wavelength of 390 m.

Absolute turbulent dissipation rates were found using the relation

$$\overline{\{w(x) - w(x+r)\}^2} = 2\varepsilon^{2/3} r^{2/3}, \tag{2}$$

where r is the separation distance and must be in the inertial subrange of the turbulence (Kaimal 1973). For each dissipation measurement the left-hand side of (2) was calculated for 2.75 m $< r <$ 200 m and plotted against $r^{2/3}$ which in almost all cases gave a straight line as expected for r in the inertial subrange. The gradient of the line was used to obtain a value of the dissipation rate ε. Mean values calculated from two or three runs using this method are plotted on a logarithmic axis in Fig. 14 for four height ranges as functions of x'. The largest dissipation rates are found in the convective boundary layer. A roughly exponential decrease $\varepsilon = \varepsilon_0 \exp(-x'/x_\varepsilon)$ is found with increasing distance seaward of the leading edge of the front. The dashed lines represent exponential fits to the data for $x' > 0$. Values of the dissipation at $x' = 0(\varepsilon_0)$ and the e-folding decay distance x_ε derived from the data are plotted as functions of height in Fig. 15. At 600 m and above the dissipation is smallest and decreases rapidly with distance seawards of the frontal edge. Below this height both the dissipation magnitude and decay distance increase as a result of additional production of turbulent kinetic energy at the sea-breeze front. At $z = 200$ m the e-folding distance has increased to around 8 km.

(*e*) *Integral scales and turbulent fluxes*

The integral scale λ_f is an important parameter in the description of turbulence and is defined, for a given spatial series $y = f(x)$, as the integral over all separation distances of the autocorrelation function of f. It is thus a measure of the horizontal eddy scale and is proportional to the power spectral peak wavelength. Lenschow and Stankov (1986) find that the vertical wind integral scale, i.e. λ_w where $f = w'(x)$, is a function of height and boundary-layer depth only for a wide range of convective boundary layers (CBLs) studied. Integral scales were calculated from the vertical wind time series for

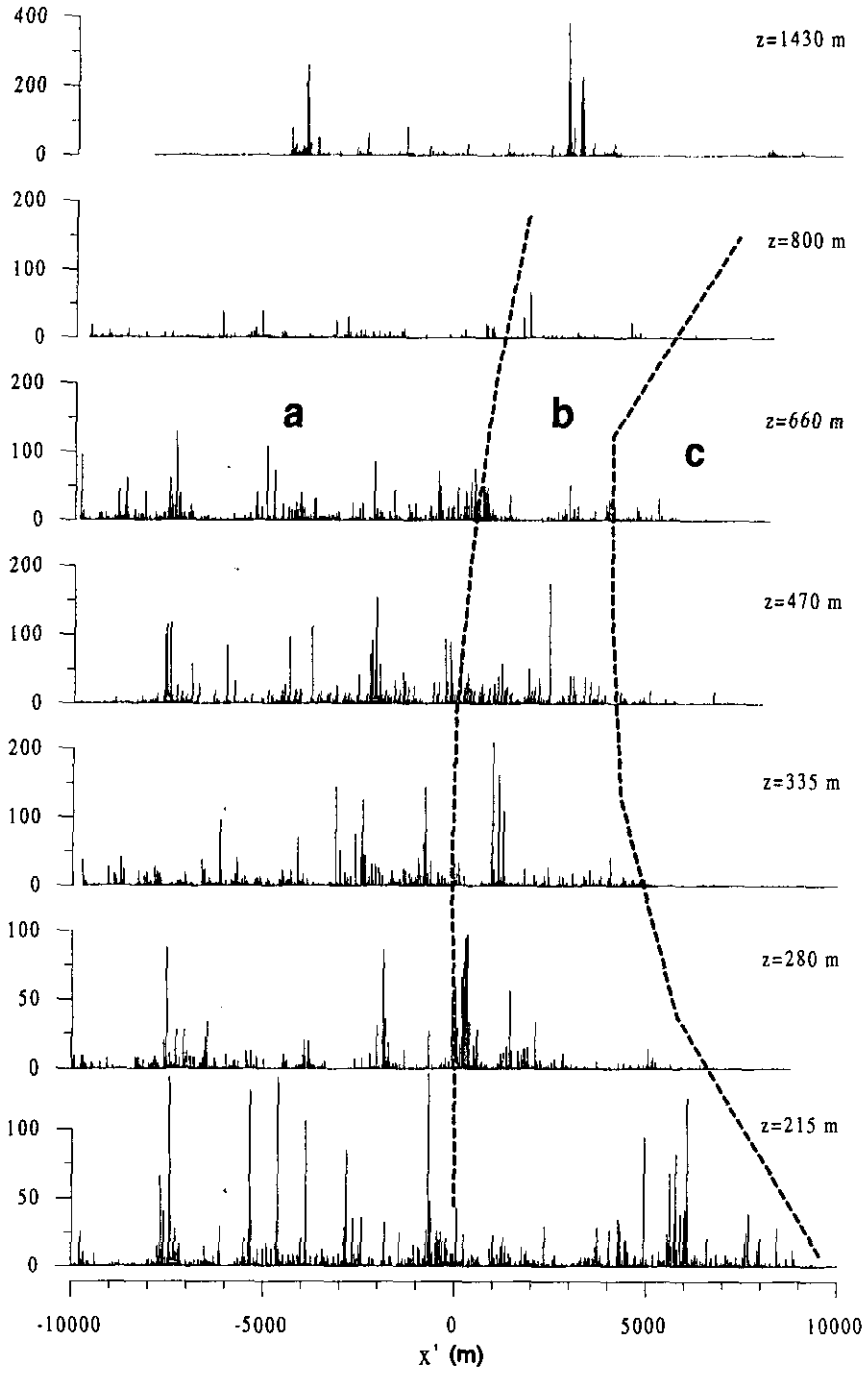

Figure 13. Aligned spatial series of $\chi/\overline{\chi}$ (see text) corresponding to the seven runs of Fig. 7. The fluctuations, calculated from the vertical wind time series, show the highly intermittent nature of the turbulence field at high frequencies. Large values are found in the convective boundary layer 'a' and in the head region 'b' where turbulence is maintained by strong shear at the boundary between the land and sea air. Much smaller values are found above the inflow region 'c' where the turbulence has decayed significantly.

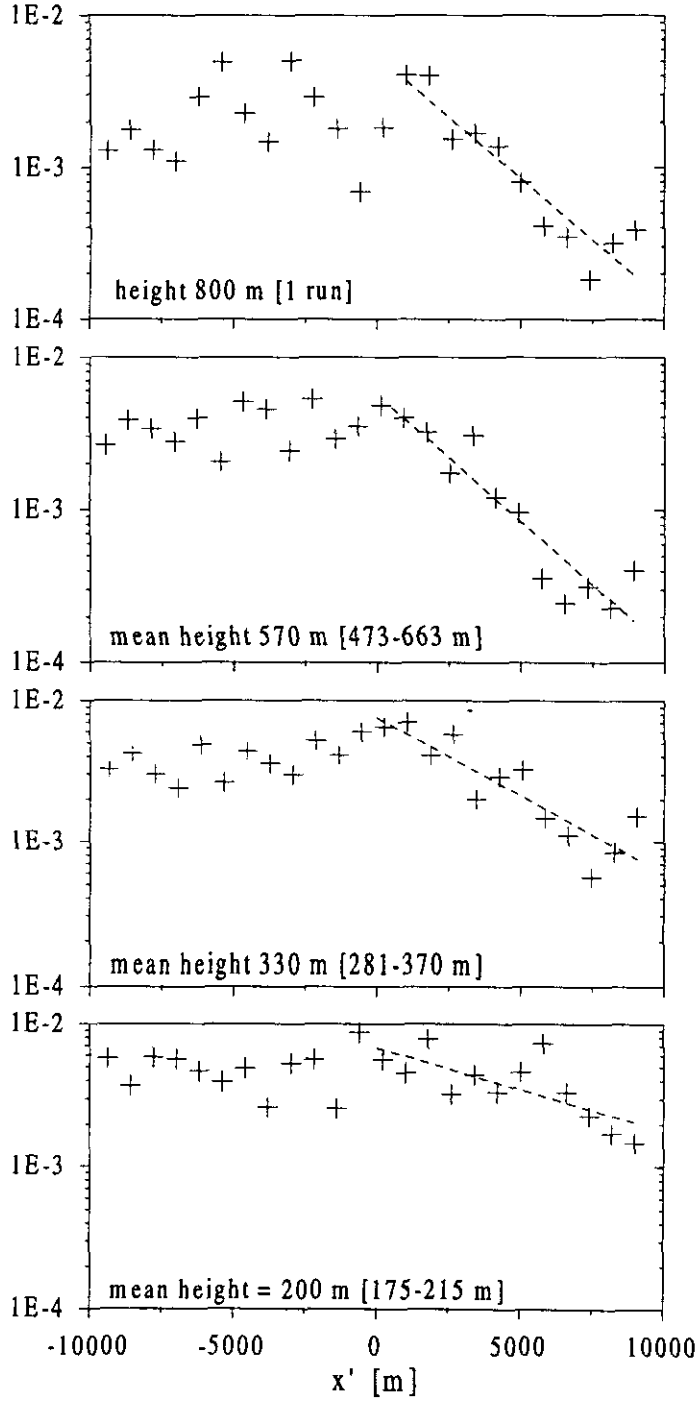

Figure 14. Dissipation values (m^2s^{-3}) as functions of x' (see text) for the sea-breeze of 25 June 1996. Dissipation values, ε, were obtained for 800 m horizontal sections of each run and then averaged to give four height ranges. The square brackets indicate the maximum and minimum run heights for each height range. Values in the convective boundary layer are roughly constant with distance landward from the front at $x' = 0$. The results suggest an exponential fall-off in dissipation seaward of the leading edge of the front.

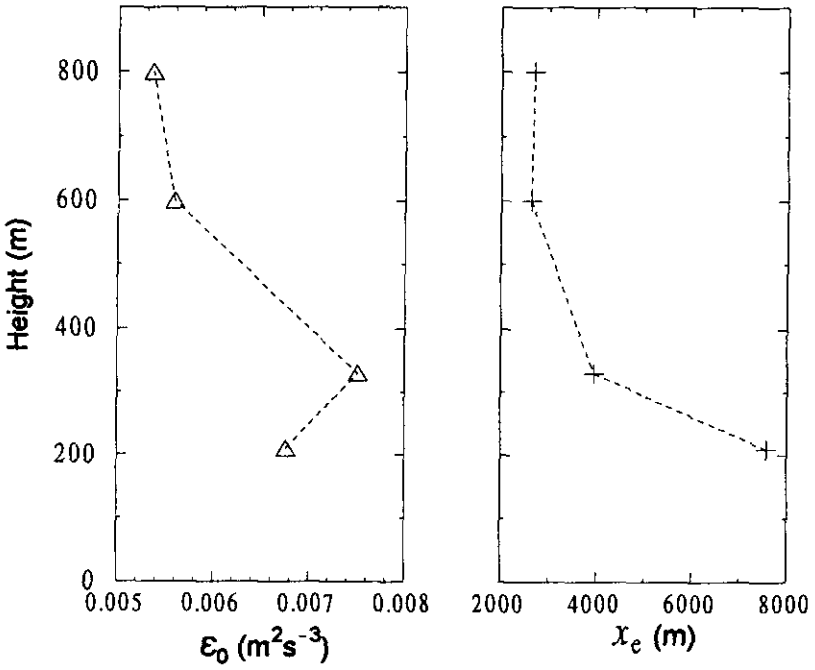

Figure 15. Values of ε_0 and x_ε (see text) from the exponential fits to the dissipation data of Fig. 14 as functions of height. Above 600 m the e-folding distance x_ε is small showing that the turbulent motions being carried seawards by the offshore wind decay very rapidly above the sea-breeze front. The e-folding distance is much greater below this layer where shear generation of turbulence at the head of the sea-breeze front maintains high dissipation rates. The largest dissipation rates at the leading edge of the front, ε_0, are found at 300 m and below.

the data on 25 June 1996 in the CBL and the sea-breeze head region. The results are plotted as a function of height in Fig. 16. The error bars are the standard deviation of the values if the data point represents an average over a number of runs. The integral scale measurements in the CBL are in very good agreement with the parametrization based upon the measurements of Lenschow and Stankov (1986). The integral scale of the turbulence increases with distance from the surface. Integral scales in the sea-breeze head region are significantly smaller than those in the CBL but approach similar values at $z = 800$ m. Turbulent mixing in the head region of the sea-breeze front occurs on scales smaller than those in the CBL at the corresponding level. Figure 17 shows the average power spectral density ($kS_w(k)$) as a function of horizontal wave number k ($= 1/\text{wavelength}$). The spectrum has a clear narrow-band peak at a wave number of around 0.003 m^{-1} corresponding to a wavelength of 330 m. This indicates the presence of unstable K–H waves on the scale of a few hundred metres. The power spectral density is larger at smaller wave numbers but the accuracy of the power-spectral estimates are poor for these wave numbers because they correspond to horizontal scales similar to the length of the series used. The power spectrum at wave numbers greater than 0.003 m^{-1} is suggestive of a turbulence cascade which appears to flatten off for wave numbers less than around 0.01 m^{-1} (100 m). The value of $kS_w(k)$ as $k \rightarrow 0.01^+$ m approaches a value of 70–100 m which is consistent with the integral scale determined using the method of *Lenschow and Stankov (1986)* described above.

Vertical-velocity variances, sensible-heat flux and front-normal vertical momentum flux were calculated using an eddy correlation technique for (a) the CBL, (b) the head

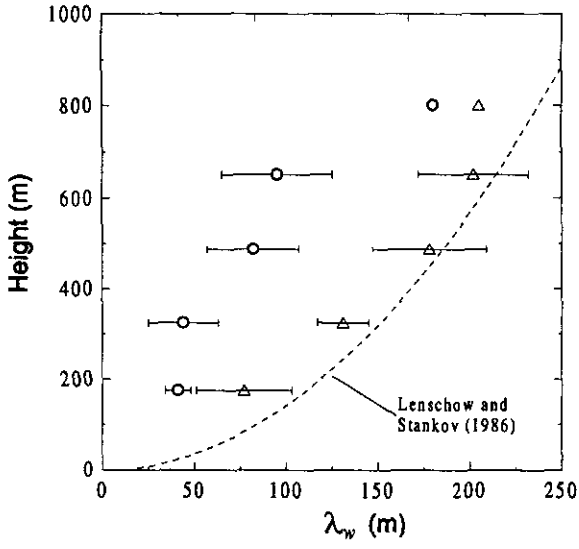

Figure 16. Vertical velocity integral scale (λ_w) measurements as functions of height. The triangles represent mean values landward of the front which agree fairly well with the measurements of Lenschow and Stankov (1986) in the convective boundary layer (CBL). The filled circles are mean values in the head region of the sea-breeze front on 25 June 1996. The integral scale is at all heights less than the corresponding integral scale in the CBL although at 800 m, above the influence of the sea-breeze, the values are similar.

region and (c) the inflow region, and are shown as functions of height in Fig. 18. The error bars are random sampling errors derived from integral scale measurements using the technique of Lenschow and Stankov (1986). In the CBL ahead of the sea-breeze front the vertical heat flux is greatest close to the surface and decreases with height to zero at around 700 m height, becoming slightly negative below the inversion. This is typical for summertime boundary layers. The convective velocity scale $w_* = (gz_i\overline{w'\theta'}/\overline{\theta})^{1/3}$, where z_i is the inversion height, is estimated to be 1.3 m s^{-1}. The largest values of the variance of the vertical wind are found at around $z = 700$ m. The along-wind momentum flux is generally positive below 750 m but the values are small and the errors fairly large. A negative momentum flux is found at $z = 800$ m which may be a result of gravity-wave activity shown in Fig. 9 and discussed in section 3(c). In contrast, the heat flux in the head region of the front is negative (≈ -0.03 K m s^{-1}) and roughly constant between $z = 250$ m and $z = 700$ m, reflecting the entrainment of warm air aloft into the cold sea air below. At $z = 800$ m the heat flux is positive, which is probably a consequence of the enhanced frontal updraught moving warm air from the CBL upwards over the frontal edge. The vertical wind variance is greatest at $z = 500$ m and decreases considerably above this height, reflecting that the greatest values of turbulent kinetic energy (TKE) are found at the cold-air/warm-air boundary where shear generation can counteract the damping effects of static stability. Momentum fluxes are negative at all levels up to the inversion in the head region as a result of a transfer of energy from the mean motion to TKE in the shear atop the cold air. It is unlikely that these negative momentum fluxes are generated by surface shear given the low value of the mean wind and the fact that there appears to be a peak in the momentum flux profile in the head region at around $z = 500$ m. The peak in the power spectrum for the head region ($200 < z < 600$ m) clearly demonstrates that K–H waves are present and it is possible that the turbulence at wave numbers greater than 0.01 m^{-1} is generated from the breaking of these waves.

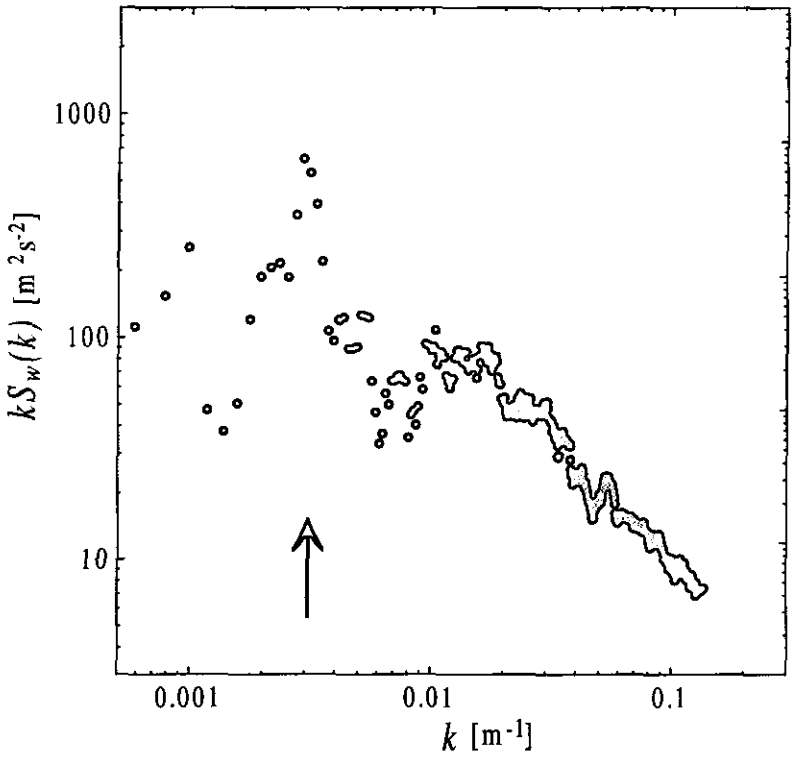

Figure 17. Power spectrum, $kS_w(k)$, of the vertical wind component for the head region of the sea-breeze front on 25 June 1996. The spectrum is an average over a number of runs in the height range $200 < z < 600$ m. The spectrum shows a peak centred on $k = 0.003$ m^{-1} (330 m wavelength). The increase in the power spectrum at scales larger than this peak is likely to arise from gravity waves.

In the inflow region no clear trend can be seen in the data. Vertical wind variances are much smaller than those in the CBL and the head region.

(*f*) *TKE budget*

The steady-state TKE budget equation, neglecting pressure transport and shear generation in a direction parallel to the line of the front (i.e. the y-direction), is

$$-\frac{g}{\bar{\vartheta}}(\overline{w'\vartheta'}) + \varepsilon = -\overline{u'w'}\left(\frac{\partial \bar{u}}{\partial z}\right) - \frac{\partial(\overline{w'e'})}{\partial z} - \frac{\partial(\overline{u'e'})}{\partial x}, \tag{3}$$

where e' is the TKE fluctuation and ε is the dissipation rate. The first term on the left-hand side (LHS) is the buoyancy production/loss (BPL) and the second term on the LHS is the loss of TKE to heat through dissipation (D). The first term on the right-hand side (RHS) is the shear production (SP) and the second and third terms on the RHS are the vertical and horizontal TKE transport terms respectively.

The TKE budget was calculated for the head region of the sea-breeze front for the two distinct height ranges: (i) 200 m $< z <$ 500 m; and (ii) 500 m $< z <$ 800 m. These were chosen because they appear to have different mean thermodynamic properties as shown in the profiles from Fig. 10. BPL, SP and D contributions for the two regions are given in Table 1. The transport terms were not calculated explicitly because, given the short lengths of data available, the errors were estimated to be several times larger

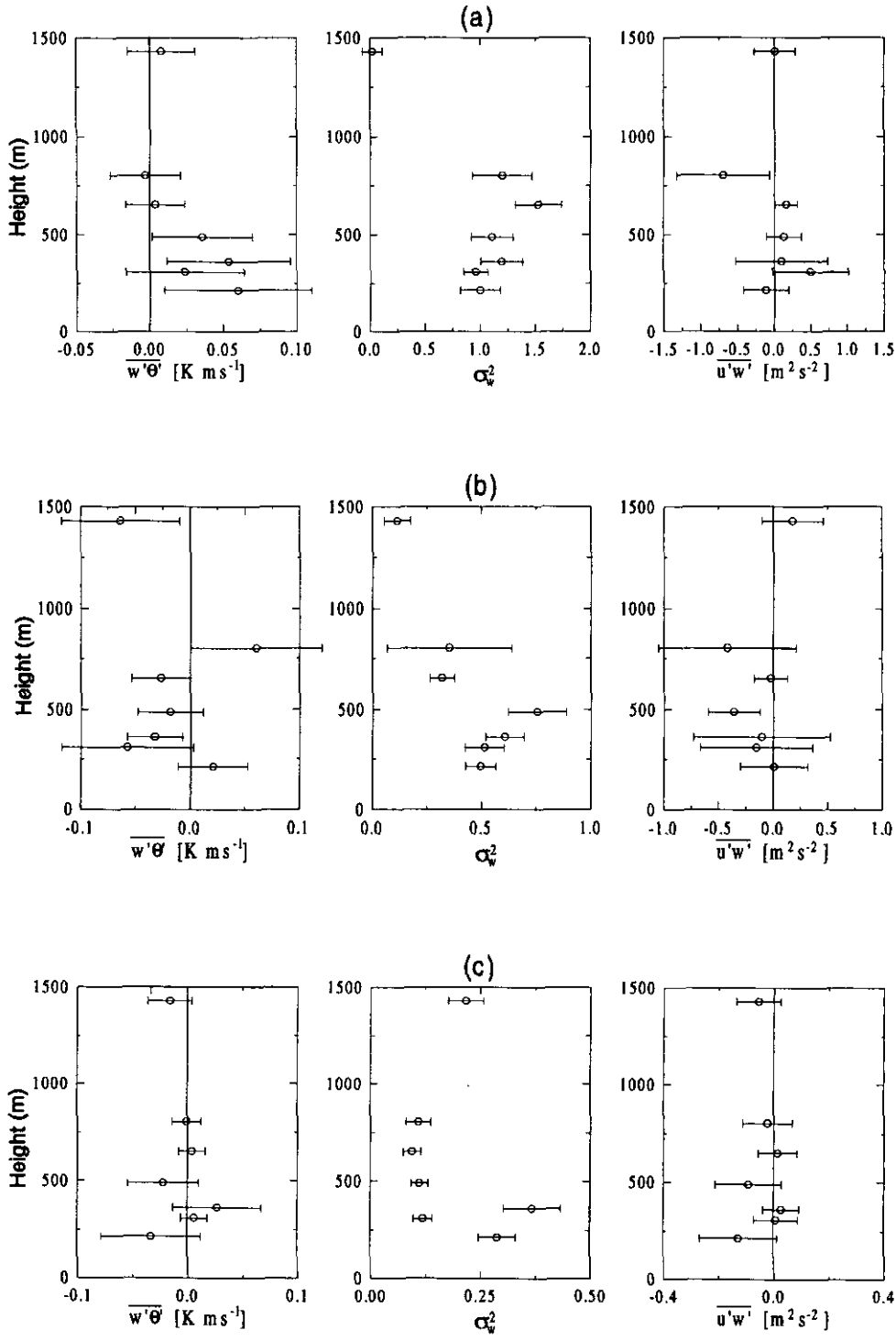

Figure 18. Sensible-heat flux ($\overline{w'\theta'}$), vertical-velocity variance (σ_w^2) and front-normal vertical momentum flux ($\overline{u'w'}$) for (a) the convective boundary layer, (b) the head region and (c) the inflow region as functions of height above the surface. See text for further explanation.

TABLE 1. CONTRIBUTIONS OF BUOYANCY (BPL), SHEAR (SP) AND DISSIPATION (D) TO THE TURBULENT KINETIC ENERGY BUDGET IN THE TWO REGIONS OF THE HEAD OF THE SEA-BREEZE ON 25 JUNE 1996

Region	BPL	SP	D	Residual
	($\times 10^{-3}$ m^{2}s^{-3})			
$200 < z < 500$ m	-0.74 ± 0.42	3.78 ± 1.97	-2.41 ± 0.89	0.63 ± 2.20
$500 < z < 800$ m	-0.87 ± 0.61	1.63 ± 0.94	-1.20 ± 0.57	-0.44 ± 1.26

z = height.

than the values themselves. The residual is the sum of BPL, SP and D. It is clear that in both regions the shear production clearly outweighs the buoyancy loss. The dissipation in both regions is roughly $0.6 \times$ SP. In the lower layer the flux Ri (−BPL/SP) is approximately 0.2, which is characteristic of turbulence generated by stable shear flows which adds weight to the hypothesis that the turbulence in the head region of the sea-breeze front is indeed generated by the vertical shear in the mean wind. The buoyancy loss is approximately equal in both regions suggesting that the mixing region extends down below the inflow height ($z = 250$ m). The residual of the three terms in the higher region is negative and significantly less than each of the three terms. In the lower region the residual is positive and comparable in magnitude with the buoyancy loss. This could be a result of advection of TKE into the upper region from the CBL, or that the turbulence created by the shear in the lower level has been transported upwards into the upper level, although the large errors in the residuals preclude confirmation of this hypothesis. The pressure-distribution term of the TKE budget equation might also be significant due to the appreciable density gradients at the top of the cold air, although it was not possible to calculate this term from the data.

4. CASE B–12 JULY 1995

(*a*) *Synoptic situation and boundary-layer profiles*

Convective conditions were prevalent during the daytime of 12 July 1995. Temperatures were high between the Midlands and the east coast where maxima of 27–28 °C were observed. Winds were light and variable in most places. Around the east coast in the afternoon the winds on the east coast acquired an offshore component of 3–4 m s^{-1}, which is favourable for sea-breeze frontal formation. A sea-breeze front formed very late in the day, at around 1630 h, and moved slowly inland, marked by a line of small cumulus and curtain cloud. By this time the convection was declining and the cumuli that had extended over much of northern England were dissipating.

Profiles were taken at 1845 h over the coast at Bridlington, and at 1735 h and 1945 h at Dishforth well to the landward side of the sea-breeze front, and are shown in Fig. 19. The landward profile at 1945 h shows a mixed layer above 500 m with approximately constant potential temperature. Below 500 m a stably-stratified layer had formed during the course of the flight as is shown in the central graph in Fig. 19. The seaward profile is similar to the landward profile above 500 m and the small differences in temperature here are not considered to be significant. At 250 m there is a sharp decrease in temperature of around 2 degC, reflecting a cold inflow of sea air. Between 250 m and 350 m there appears to be an unstable layer with a stable layer between 350 m and 500 m. The seaward profile on 25 June 1996 (Fig. 3) shows a stable layer below 400 m with a sharper drop in temperature at around 250 m. Apart from the peak in temperature at 275 m, the structure on 12 July below 400 m is broadly similar to that

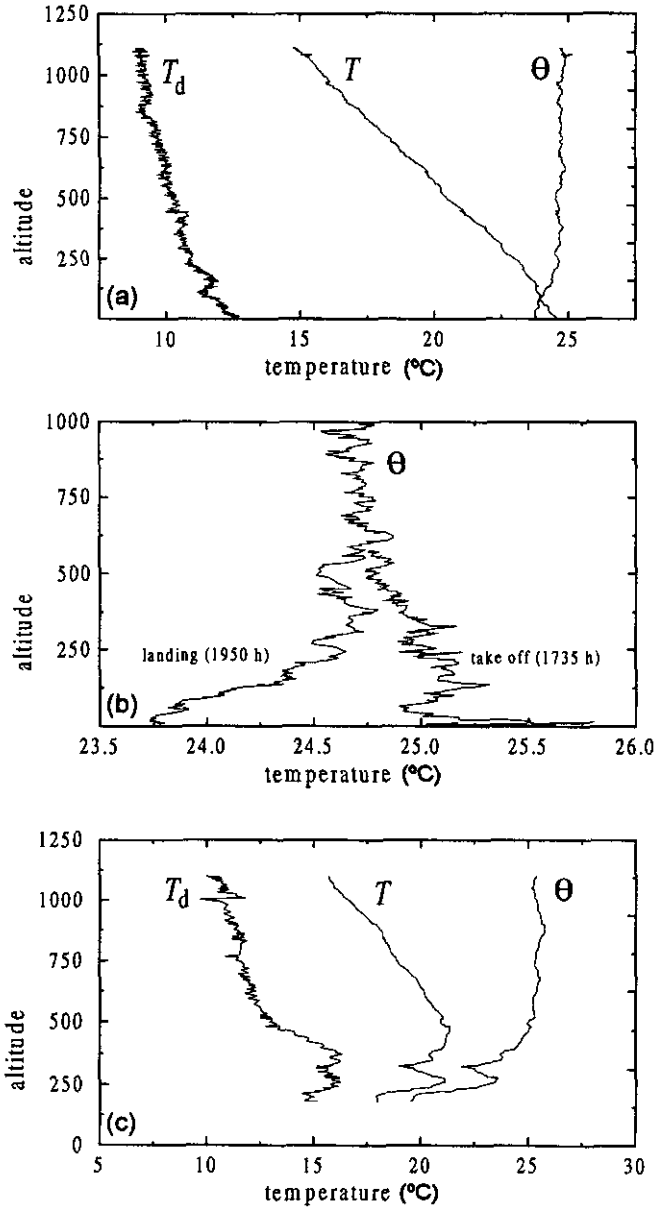

Figure 19. Profiles of temperature (T), potential temperature (θ) and dew-point (T_d) taken on 12 July 1995 at (a) Dishforth airfield (landward of the front at 1945 h) and (c) close to Bridlington (seaward of the front at 1845 h). The effect of the cold sea-breeze on the boundary layer below 500 m is clearly seen on the seaward profile. (b) Shows the change in the stability of the lower boundary layer between 1735 h and 1950 h at Dishforth as the convective boundary layer is decaying and a stably-stratified layer forms. Altitudes are metres above mean sea level.

on 25 June 1996, suggesting that the peak may be caused by an entrainment event of warm air into the sea-breeze, temporarily altering the profile. A boundary layer capping inversion was observed at 1400 m by the Meteorological Research Unit tethered balloon situated around 10 km from the coast along the track of runs 1–4.

The sea-breeze was marked by a bank of cumulus aligned parallel to the coastline around 15 km inland. Ragged curtain cloud with a lower cloud base than the cumulus,

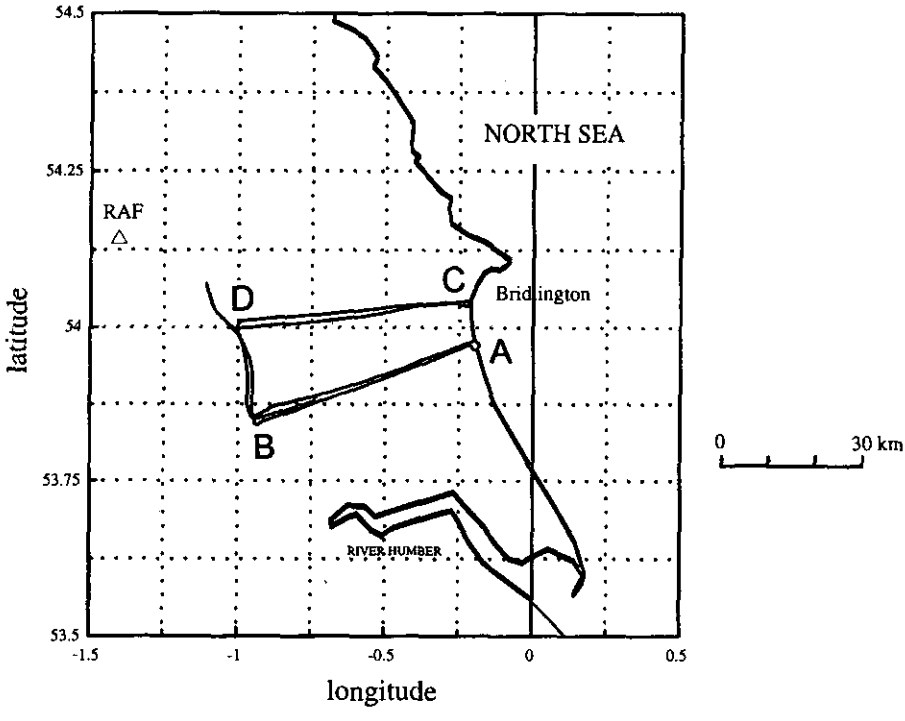

Figure 20. Aircraft flight tracks for 12 July 1995.

formed as the moist, cool sea air was forced upwards at the front, was also observed. The seaward-side of the front was cloudless. Four runs were made along the line AB (Fig. 20) and two runs along the line CD around 20 km to the north.

(*b*) *Spatial series, cross-sections and vertical structure*

The method described in section 3(c) was used to align runs 1–4 onto a front-relative coordinate x'. Two runs at $z = 540$ m and $z = 570$ m were used to obtain the speed of 1.62 m s^{-1} for the front. Aligned spatial series of vertical velocity, potential temperature, specific humidity and front-normal wind speed are shown in Fig. 21. The front is clearly shown by the sharp gradients in temperature and specific humidity around $x' = 0$. The frontal updraught varies from a sharply defined region 2500 m wide with vertical velocity of around 2.5 m s^{-1} (run at $z = 540$ m) to a diffuse updraught region, 5000 m wide, with vertical velocities of around 1.5 m s^{-1} (run at $z = 570$ m). These two runs were closely spaced in altitude with frontal crossings separated by around 12 minutes in time and so it is clear that the frontal dynamics are changing rapidly in time. No clearly-defined frontal updraught can be seen at $z = 1225$ m, and there is no corresponding rise in specific humidity, suggesting that the sea-breeze front is confined to lower altitudes. During the course of the runs, a period of roughly 45 min, a decrease in the strength of the boundary-layer convection was noted by the pilot. The variance of the vertical velocity to the landward side of the front fell from 0.73 m^{2}s^{-2} on run 3 (570 m) to 0.26 m^{2}s^{-2} on run 4 ($z = 540$ m); on run 6 ($z = 630$ m), made 50 min after run 3, a distance 20 km to the north of runs 1–4, the vertical-velocity variance had reduced still further to 0.12 m^{2}s^{-2}. Similarly, the standard deviation of wind speed,

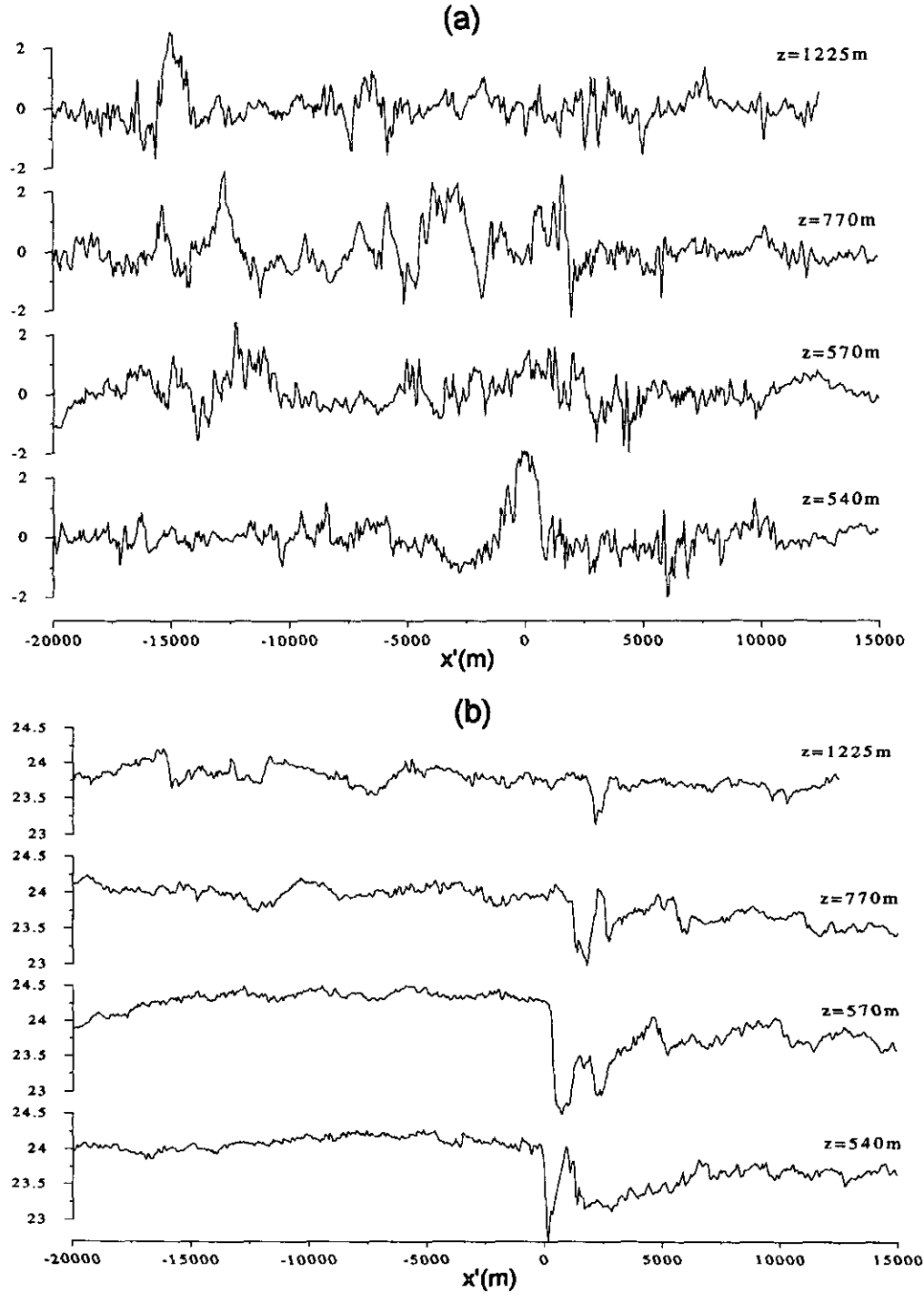

Figure 21. Aligned spatial series of (a) vertical velocity (m s^{-1}), (b) potential temperature (°C), (c) specific humidity (g kg^{-1}) and (d) front-normal wind speed (m s^{-1}) (positive for offshore) from four of the aircraft runs along the line AB (see Fig. 20) on 12 July 1995.

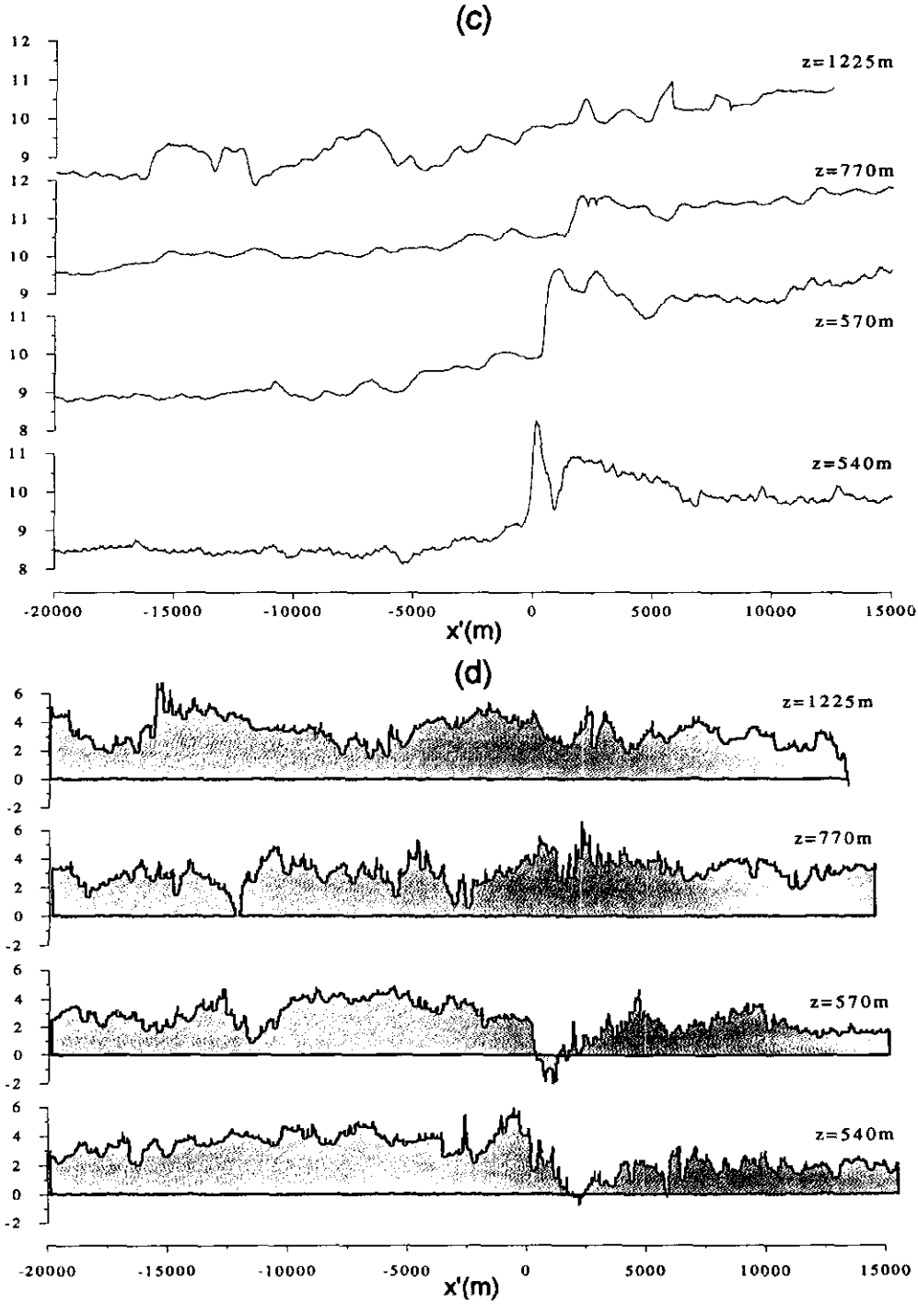

Figure 21. Continued.

expressed as a fraction of the mean, is 0.27 on run 4, 0.21 on run 5 and 0.13 on run 6. The clearly defined frontal updraught on run 4 is most likely a result of the fact that the front is moving into more stable air as the convection wanes and there is less modification of the frontal updraught by convective cells.

Two runs were carried out around 20 km to the north of the first four runs. Spatial series of wind speed perpendicular to the front, vertical wind component, potential temperature, specific humidity, $\overline{w'\theta'}$ and $\overline{u'w'}$ are shown for a run at $z = 630$ m in Fig. 22. The covariances were calculated by high-pass filtering of the spatial series with a moving-average filter with a width of 4 km and are shown in grey. The black line through the flux data is a 1 km wide moving-average smoothing of the flux data. The raw vertical velocity data are shown in grey and with smoothing (again 1 km moving average) in black. It is clear that there is much less turbulence by this time, and the peak vertical velocity is less than 1 m s^{-1}. Sharp gradients of temperature and specific humidity are seen in the data at 630 m. On the final run of the four southerly runs, the front was crossed at 1844 h, a distance of 22.5 km from the coast at point B. On the final run, the first sharp drop in temperature moving seawards was crossed at 1922 h, a distance of 29.8 km from the coast at point C. Although the two runs were separated laterally by around 20 km, these data suggest that the front had accelerated to a speed of the order of 3 m s^{-1}. One could argue that the data are insufficient to make this statement, given the lateral spatial separation of the runs. However, given that the front was passing over flat terrain in the region of runs 1–4 and had been moving uphill between points C and D, this suggests that there had been a definite acceleration of the front. It is possible that the frontal speed increased as the turbulence decreased (from the stronger convective activity earlier in the day) in the region into which it was flowing, although the absence of measurements earlier in the day makes this impossible to confirm. Such an acceleration is supported by a study of the rate of advance of a front by Simpson *et al.* (1977) which showed that the speed of the front increased markedly as the solar-heat flux at the surface decreased. No specific reference in this case was made to the turbulence in the boundary layer, but as the turbulence is driven by the surface solar-heat flux, it is likely that the reduction in turbulence would increase the speed of the front, by a reduction of the turbulent erosive detrainment of cool air out of the sea-breeze.

More interesting still is that the temperature and specific humidity seaward of the initial sharp jump, oscillate in a sawtooth manner, with five discernible and coherent sharp increases in humidity (drops in temperature) and rather less sharp drops, with the wavelength increasing from around 1000 m close to the initial jump to around 3000 m further back from the front. The physical reason for the waves is not known. One hypothesis, that the waves are in fact a train of K–H billows, could be incorrect because the wavelength appears to be too long. If the waves were indeed K–H billows then the layer of $Ri < 0.25$ would have to be (Turner 1973) around 150 m thick close to the first temperature/humidity jump, increasing to around 450 m thick seawards of the initial jump. Observations of the front on 25 June 1996 suggest that the wavelength would be of the order of hundreds of metres rather than several kilometres. Unfortunately, it was not possible to carry out such a detailed profile analysis for this dataset given the limited number of runs.

A second hypothesis for the curious coherent disturbances is that the waves were some form of solitary wave formed as the sea-breeze interacts with an early evening stable boundary layer close to the surface. The profile in Fig. 19 shows that such a boundary layer had established itself between take-off (1735 h) and landing (1950 h). Several different types of solitary wave have been shown to propagate on shallow

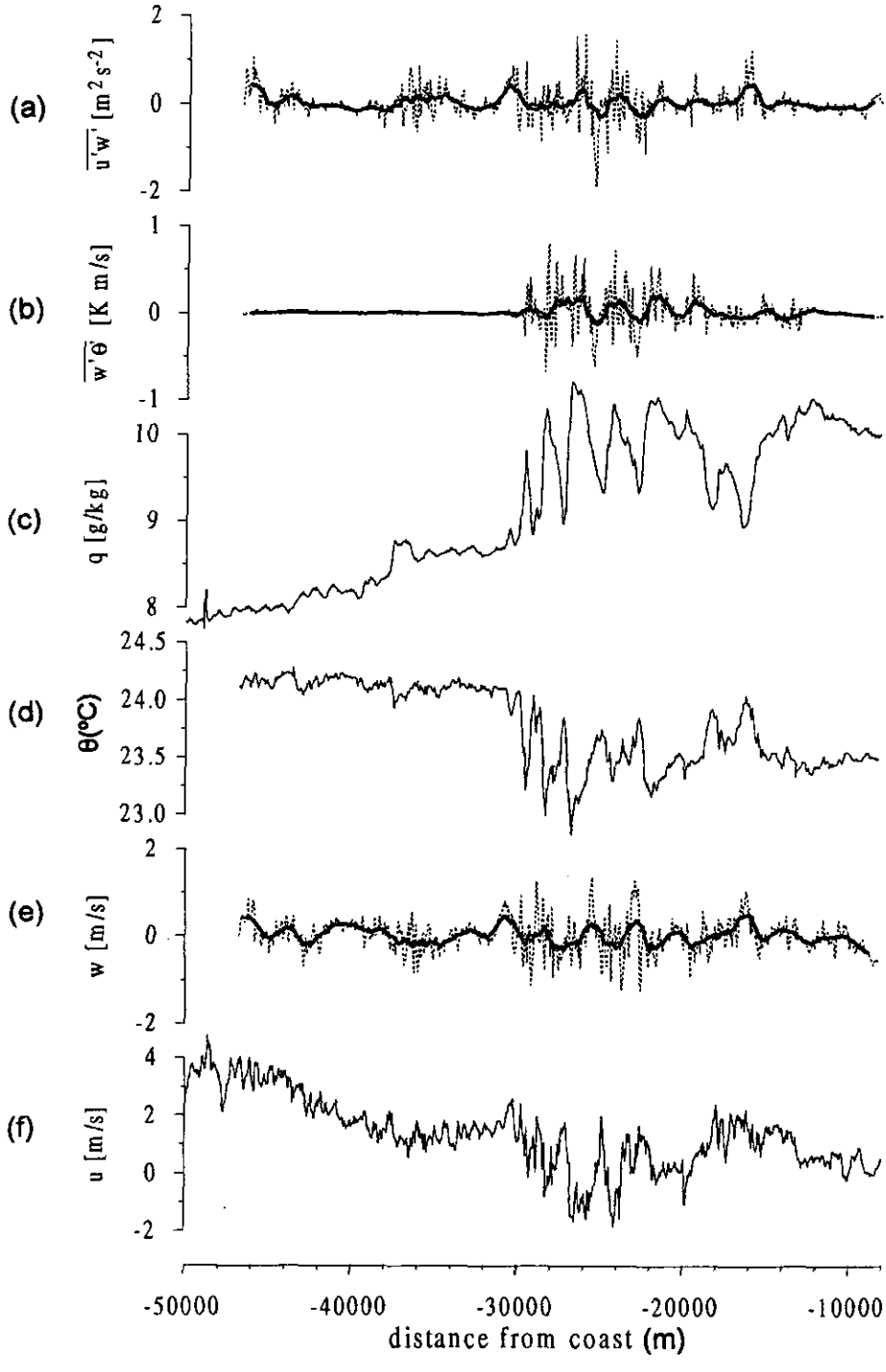

Figure 22. Spatial series of (a) $\overline{u'w'}$, (b) $\overline{w'\theta'}$, (c) specific humidity, (d) potential temperature, (e) vertical wind component and (f) wind speed perpendicular to the front for a run at $z = 630$ m along the line CD (see Fig. 20) on 12 July 1995. The covariances were calculated by high-pass filtering of the spatial series with a moving-average filter with a width of 4 km and are shown in grey. The black line through the flux data is a 1 km wide moving-average smoothing of the flux data.

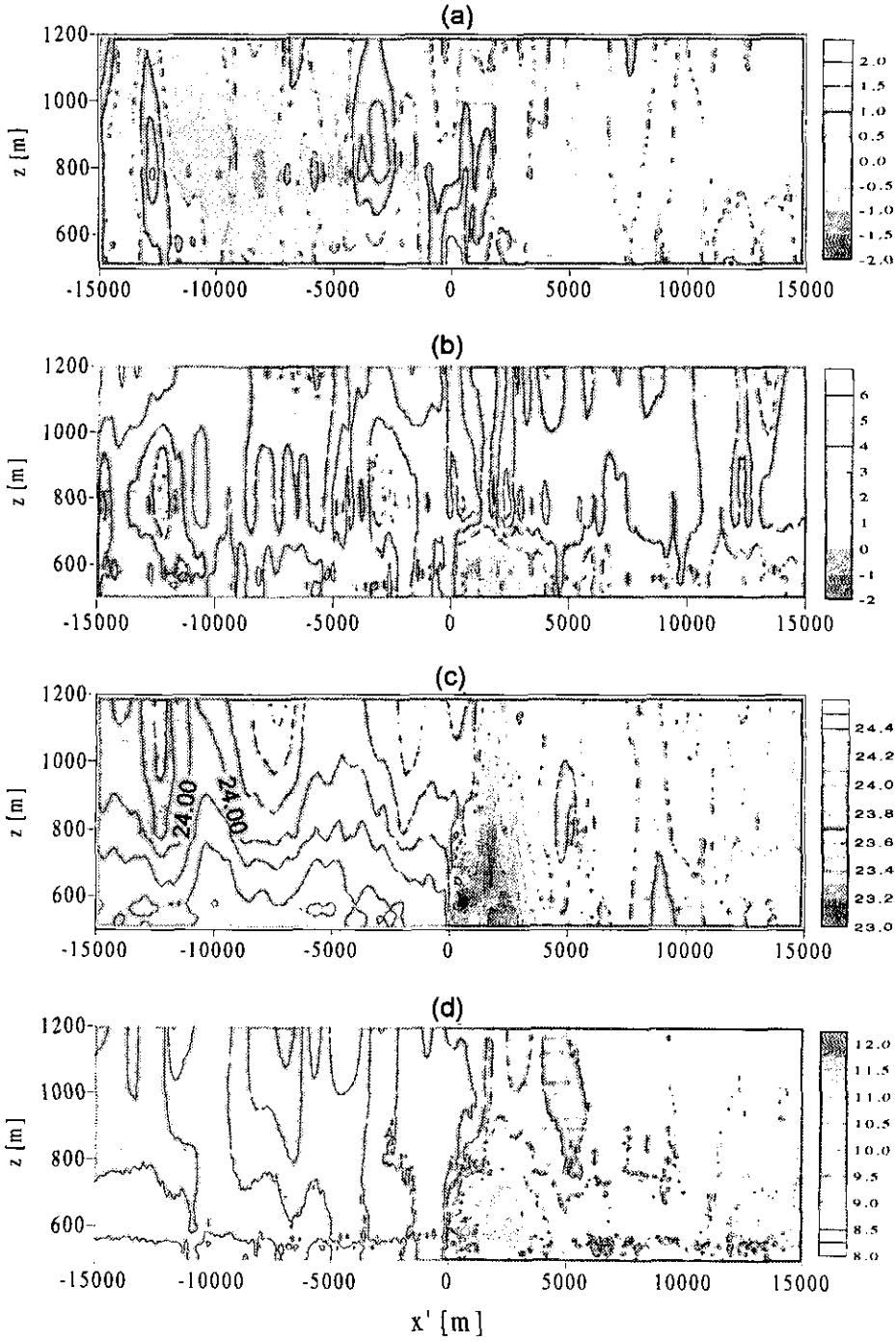

Figure 23. Cross-sections of (a) vertical velocity (m s^{-1}), (b) front-normal wind speed (m s^{-1}), (c) potential temperature (°C) and (d) specific humidity (g kg^{-1}) from the four runs along AB (see Fig. 20) on 12 July 1995.

nocturnal inversions (Christie *et al.* 1981; Christie and Muirhead 1981), and atmospheric density currents (Christie *et al.* 1979), and solitary waves have been studied in laboratory tank models (Maxworthy 1980). Essentially, the interaction of an intrusive density current with a stable layer of the atmosphere triggers the production of a series of sharply defined non-dispersive waves which propagate along the stable layer. A closed circulation is often found within each wave, so that in the case of a sea-breeze, a previously connected sea-breeze intrusion can become a series of separated vortices which travel at a speed greater than the original speed of the front. The wave train in Fig. 22 resembles in structure waves observed with a microbarograph array by Christie *et al.* (1981) which had been caused by an intrusive gravity current in that the waves are ordered by amplitude, which is seen in the humidity series in Fig. 22. Further evidence for the postulation that these waves are indeed solitary is offered by the modelled evolution of solitary waves from a single intrusive current. Nonlinear dispersive wave theory suggests that an initial disturbance will form at the leading edge of the density current. Subsequently, solitary waves will emerge as the wave propagates. The spatial series of temperature and humidity at $z = 540$ m (Figs. 21(b) and (c)) clearly show a sharp disturbance at the leading edge of the main sea-breeze disturbance. This may be the initial development of a solitary wave train. If the waves are indeed solitary in nature, and occur regularly with sea-breezes as the daytime CBL is replaced by a stable layer, it might offer an explanation for the reported occurrences of sea-breezes penetrating hundreds of kilometres inland, and increasing their speed in the process. It has been suggested that the sea-breeze cut-off vortex studied by Simpson *et al.* (1977) is in fact the first of a series of propagating solitary waves.

Cross-sections of vertical and horizontal wind component, potential temperature and specific humidity were produced from the four runs aligned along AB and are shown in Fig. 23. Although the data are more sparse in the vertical than for the 25 June 1996 flight several important features are resolved, although some distortion of the cross-sections is likely due to the rapid changes associated with the onset of the early-evening boundary layer. First, the raised head of the cold sea-breeze is clearly seen, with a corresponding coherent updraught region to the landward side. The head extends to a height of around 700 m as shown by the front-normal wind-speed component. The potential temperature and specific humidity cross-sections, however, indicate that a cold, moist region extends up to around 1200 m. Why the humidity and potential-temperature structure differ markedly from the horizontal wind structure is not known. Second, the convective activity landward of the front is not present in the air above the sea-breeze. Third, the potential-temperature field landward of the front (-15 km $< x' < 0$ km) appears to show some wave activity with a horizontal wavelength of 3–5 km, although the wave amplitude is small. Fourth, the offshore wind speed does not increase above the sea air. The Froude number estimated from (1) is, given the accuracy of the measurements, between 0.60 and 0.80, suggesting that the flow is largely subcritical.

(c) *Fluxes of heat and momentum and the TKE budget*

Fluxes of sensible heat and vertical flux of momentum were calculated for runs 1–4 using the same criteria for separating the runs into boundary-layer sections, head sections and regions seaward of the head region using the method used in section 3(f). The sensible-heat fluxes measured for the four runs are shown in Table 2.

The heat fluxes in the boundary layer ahead of the front are small in magnitude, reflecting the reduction of convective motions in the early evening. The convective velocity scale is estimated to have a value $w_* = 0.6$ m s^{-1}. The sensible-heat fluxes in the head region of the front are negative other than for run 4. In the region seaward

TABLE 2. SENSIBLE-HEAT FLUXES MEASURED ON RUNS ALONG AB (SEE FIG. 1) ON 12 JULY 1995, FOR THE CONVECTIVE BOUNDARY LAYER (CBL), THE HEAD REGION AND THE REGION SEAWARD OF THE HEAD REGION

Height (m)	$\overline{w'\theta'}$(K m s^{-1})		
	CBL	Head	Seaward
1225	-0.009 ± 0.005	-0.010 ± 0.009	0.005 ± 0.003
770	0.004 ± 0.003	-0.014 ± 0.016	0.006 ± 0.004
570	0.006 ± 0.004	-0.033 ± 0.012	-0.008 ± 0.004
540	0.003 ± 0.002	$+0.009 \pm 0.011$	0.003 ± 0.003

TABLE 3. VERTICAL FLUX OF FRONT-NORMAL MOMENTUM MEASURED ON RUNS ALONG AB (SEE FIG. 1) ON 12 JULY 1995, FOR THE CONVECTIVE BOUNDARY LAYER (CBL), THE HEAD REGION AND THE REGION SEAWARD OF THE HEAD REGION

Height (m)	$\overline{u'w'}$(m^{2}s^{-2})		
	CBL	Head	Seaward
1225	0.14 ± 0.14	-0.05 ± 0.11	0.10 ± 0.20
770	-0.24 ± 0.21	-0.08 ± 0.09	0.01 ± 0.13
570	-0.26 ± 0.19	-0.52 ± 0.34	-0.07 ± 0.10
540	-0.49 ± 0.28	-0.46 ± 0.44	-0.02 ± 0.11

TABLE 4. CONTRIBUTIONS OF BUOYANCY (BPL), SHEAR (SP) AND DISSIPATION (D) TO THE TURBULENT KINETIC ENERGY BUDGET IN THE HEAD REGION OF THE SEA-BREEZE ON 12 JULY 1995

Region	BPL	SP	D	Residual
	($\times 10^{-3}$ m^{2}s^{-3})			
$500 < z < 800$ m	-0.43 ± 0.46	3.21 ± 2.95	-2.60 ± 1.25	$+0.18 \pm 3.22$

z = height.

of the head region the fluxes are smaller in magnitude than those in the head region, comparable with those in the boundary layer ahead of the front. The mean heat flux in the head region below $z = 800$ m is -0.013 ± 0.017 K m s^{-1}.

The vertical momentum fluxes are shown in Table 3 for the four runs between points A and B. The momentum flux in the boundary layer is negative up to at least 770 m. In the head region the fluxes are small above 600 m, but below this they are greater in magnitude and negative, representing the shear production of turbulence in the head region. The momentum fluxes in the tail region are small at all levels.

The contributions to the TKE budget in the head region were derived using the runs between $z = 500$ m and $z = 800$ m. The vertical wind shear, estimated from the cross-section of wind speed, was 0.009 s^{-1}. Dissipation rates were calculated from the vertical velocity structure function. The results are shown in Table 4, for the contributions from SP, BPL and D. The major contribution to the TKE budget is SP, which exceeds BPL by a factor of 7.5. The residual is small in comparison with the other terms, leading to the conclusion that the three terms considered in the TKE budget equation are the major contributors to TKE production and loss, and that the TKE transport and pressure transport terms are small, or at least cancel each other out.

5. Discussion

Observations of two sea-breezes have been presented. In case A (25 June 1996) the sea-breeze formed in the late morning and advanced inland into a convective boundary layer categorized by relatively strong turbulence ($w_* \approx 1.3$ m s^{-1}). In case B (12 July 1995) the sea-breeze formed much later, in the mid afternoon, and advanced into a boundary layer with significantly weaker turbulent activity ($w_* \approx 0.6$ m s^{-1}). Indeed, in case B the strength of the turbulence was decreasing during the course of the measurements. Evidence of the formation of a stable layer close to the surface was seen in a vertical profile as the aircraft landed at 1950 GMT. The offshore component of the wind speed ahead of the front was similar (3–4 m s^{-1}) in both cases. The speed of the front (at the time of the measurements) was around 1.25 m s^{-1} for case A and 1.62 m s^{-1} for case B. The greater frontal speed for case B is likely to be a result of the weaker turbulence in the air into which the front was propagating. Evidence suggests that the frontal speed increased to around 3.2 m s^{-1} as the boundary-layer turbulence weakened during the course of the measurements. The difference between the time of onset of the sea-breeze in case A (late morning) and that of the sea-breeze in case B (mid afternoon) is likely to be due to the lower coastal sea surface temperature (11–13 °C) for case A than for case B (14–16 °C) although the fact that the maximum inland temperatures for case B were 27–28 °C suggests that strong convective turbulence (before the measurement period) could be an additional (and perhaps more important) factor in the late onset of the front in this case (Reible *et al.* 1993). Although for case B the speed of the front during the measurement period was higher than for case A it may well have been much slower during the afternoon when the convective activity was stronger, and so it is difficult to account for the differences in the frontal speeds with a simple explanation, although Reible *et al.* (1993) show that the frontal speeds are generally slower when convective activity is greatest.

Cross-sections of vertical velocity, wind speed perpendicular to the front, potential temperature and specific humidity were constructed from a number of aircraft runs in a direction perpendicular to the observed line of the front as determined by a line of cumulus clouds produced from enhanced uplift at the leading edge of the front. For the case A front the aircraft runs ranged between 215 and 1430 m above the surface, while for case B the runs ranged between 540 and 1225 m above the surface. Both sea-breeze fronts consisted of a raised frontal head with a shallower inflow of sea air below. The head was extended to a height of 500–600 m for case A and around 700 m for case B. The inflow depth for case A was 300 m, and it was not possible to determine its depth from the aircraft measurements for case B, although observations from the Meteorological Research Unit balloon indicated its depth to be 300 m.

The cross-sections for case A, which were the most detailed due to the larger number of runs used, showed that the slope of the leading edge of the front was around 30° to the horizontal between the heights of 200–500 m above the surface. A frontal updraught existed which varied in both magnitude and horizontal extent as a result of the interaction with convective cells in the boundary layer, and a possible lobe and cleft structure in the leading edge of the front. For case B, the frontal updraught also occurred, and was of a similar magnitude to that of case A. Cross-sections revealed that the frontal slope was 15–20° to the horizontal, somewhat shallower than the case A front, possibly because the front was crossing flat terrain on 12 July 1995 and moving up a shallow gradient on 25 June 1996.

Evidence of Kelvin–Helmholtz instability and billows for case A was seen from an analysis of Ri profiles and from direct observations of a wave train with a wavelength of

390 m consistent with the wavelength predicted by the *Ri* analysis, which showed the expected wavelength to be between 300 m and 1000 m. Measurements of dissipation showed an approximately exponential decrease with distance seaward of the leading edge of the front, suggesting that the most intense mixing and TKE generation occurs close to the leading edge of the front.

Sensible-heat fluxes were calculated for the CBL, the head region and the tail region of inflow seaward of the head. Predominantly positive heat flux was seen in the CBL which for case A decreased from around 0.05 K m s^{-1} at $z = 200$ m to close to zero at $z = 800$ m, around 80% of the boundary-layer height. Momentum fluxes were largely positive, roughly 0.20 $m^2 s^{-2}$ below $z = 800$ m and negative above, possibly as a result of friction between air in the boundary layer and the free troposphere. The heat flux in the region of the head was negative from $z = 250$ m to around 700 m, with a mean of -0.032 ± 0.015 K m s^{-1}, with a negative momentum flux of around -0.25 ± 0.20 $m^2 s^{-2}$. In contrast, the mean sensible-heat flux in the head region was -0.013 ± 0.017 K m s^{-1}. Detrainment from the sea-breeze was considerably less for case B and this is likely to be a consequence of the reduced turbulence in the convective boundary-layer air flowing over the sea-breeze.

The inflow region in both cases showed considerably smaller values of both heat and momentum flux with no discernible height trend. Contributions of the shear, buoyancy and dissipation to the TKE budget in the head region showed that the turbulent production was greater than the buoyancy loss for case A by a factor of 5.1 between 200 m and 500 m height, and 1.8 between 500 m and 800 m. In contrast, the shear production of TKE in the head region of the front for case B exceeded the buoyancy loss by a factor of 7.5 for the 500 m to 800 m height range. The shear production in the 500–800 m height range for case B was approximately 200%, and the buoyancy production 50% of the values for case A.

Although the measurements have highlighted differences between the sea-breeze fronts in the two case-studies, uncertainty in the measurements precludes precise quantitative analysis as to the effect of turbulence on the sea-breeze. Detailed measurements are expected from the Meteorological Research Unit balloon facility for the sea-breeze on 12 July 1995 in which the tethered balloon made turbulence measurements at eight levels simultaneously.

ACKNOWLEDGEMENTS

We are grateful to the staff of the Yorkshire Gliding Club whose hospitality during the 1995 and 1996 field projects was warmly appreciated. Thanks to John Cardwell of UMIST for aircraft scientist duties on 12 July 1995. We thank also the Meteorological Research Unit of the UK Meteorological Office for their weather forecasting assistance and early warnings of sea-breeze formation. R. Wood acknowledges receipt of a studentship from the Natural Environment Research Council who also supported this project with research grant GR9/1692.

REFERENCES

Britter, R. E. and Simpson, J. E. 1978 Experiments on the dynamics of a gravity current head. *J. Fluid. Mech.*, **88,** 223–240

Christie, D. R. and Muirhead, K. J. 1981 'Observations of solitary atmospheric waves over Northern Australia'. Pp. 463–466 in Second applied physics conference, Melbourne. Australian Institute of Physics

Christie, D. R., Muirhead, K. J. and Hales, A. L. 1979 Intrusive density flows in the lower troposphere: A source of atmospheric solutions. *J. Geophys. Res.*, **84,** C8, 4959–4970

Christie, D. R., Muirhead, K. J. and Clarke, R. H. 1981 Solitary waves in the lower atmosphere. *Nature*, **293**, 46–49

Hacker, J. M., Hartmann, J., Kraus, H. and Schwerdtfeger, P. 1990 'Airborne measurements of the structure of sea-breeze fronts in summer 1988/89'. F.I.A.M.S. Research Report No. 47. *Flinders Institute for Atmospheric and Marine Sciences*, Flinders University of South Australia, Bedford Park 5042, Australia

Kaimal, J. C. 1973 Turbulence spectra, length scales and structure parameters in the stable surface layer. *Boundary-Layer Meteorol.*, **4**, 289–309

Koschmieder, H. 1936 Danziger seewindstudien, I. *Danzig Meteorol. Forsch.*, **8**

Kraus, H., Hacker, J. M. and Hartmann, J. 1990 An observational aircraft-based study of sea-breeze frontogenesis. *Boundary-Layer Meteorol.*, **53**, 223–265

Lawson, T. 1971 Haboob structure at Khartoum. *Weather*, **26**, 105–112

Lenschow, D. H. and Stankov, B. B. 1986 Length scales in the convective boundary layer. *J. Atmos. Sci.*, **43**, 1198–1209

Lenschow, D. H., Mann, J. and Kristensen, L. 1994 How long is long enough when measuring fluxes and other turbulent statistics? *J. Atmos. Oceanic Technol.*, **11**, 661–673

Liu, C. and Moncrieff, M. W. 1996 A numerical study of the effects of ambient flow and shear on density currents. *Mon. Weather Rev.*, **124**, 2282–2303

Maxworthy, T. 1980 On the formation of nonlinear internal waves from the gravitational collapse of mixed regions in two and three dimensions. *J. Fluid Mech.*, **96**, 47–64

Meneveau, C. and Sreenivasan, K. R. 1991 The multifractal nature of turbulent energy dissipation. *J. Fluid Mech.*, **224**, 429–484

Mueller, C. K. and Carbone, R. E. 1987 Dynamics of a thunderstorm outflow. *J. Atmos. Sci.*, **44**, 1879–1898

Offiler, D., Brown, P. R. A., Grant, A. L. M., Jackson, W. D. N. and Johnson, D. W. 1994 'Report of the Aircraft Winds Working Group'. MRF Technical Note 17, July 1994. Meteorological Research Flight, Building Y46, DRA, Farnborough, Hampshire, GU14 6TD, UK

Reible, D. D., Simpson, J. E. and Linden, P. F. 1993 The sea-breeze and gravity-current frontogenesis. *Q. J. R. Meteorol. Soc.*, **119**, 1–16

Sha, W. and Kawamura, T. 1991 A numerical study on sea/land breezes as a gravity current: Kelvin–Helmholtz billows and inland penetration of the sea breeze front. *J. Atmos. Sci.*, **48**, 1649–1665

Simpson, J. E. 1972 Effects of the lower boundary on the head of a gravity current. *J. Fluid. Mech.*, **53**, 759–768

Simpson, J. E. and Britter, R. E. 1979 The dynamics of the head of a gravity current advancing over a horizontal surface. *J. Fluid. Mech.*, **94**, 477–495

1980 A laboratory model of an atmospheric mesofront. *Q. J. R. Meteorol. Soc.*, **106**, 485–500

Simpson, J. E., Mansfield, D. A. and Milford, J. R. 1977 Inland penetration of sea-breeze fronts. *Q. J. R. Meteorol. Soc.*, **103**, 47–76

Wood, R., Stromberg, I. M., Jonas, P. R. and Mill, C. S. 1997 Analysis of an air motion system on a light aircraft for boundary layer research. *J. Atmos. Oceanic Technol.*, **14**, 960–968